



NTNU – Trondheim
Norwegian University of
Science and Technology

Detection of Conglomerate Formations While Drilling

Ulrikke Nilsen

Petroleum Geoscience and Engineering

Submission date: June 2015

Supervisor: Pål Skalle, IPT

Co-supervisor: Trym Elseth, Lundin Norway AS

Norwegian University of Science and Technology

Department of Petroleum Engineering and Applied Geophysics

Acknowledgement

Present work is a Master Thesis within Drilling Technology at the Department of Petroleum Technology and Applied Geophysics, at the Norwegian University of Science and Technology (NTNU). Ulrikke Nilsen carried out the work partly in Trondheim and partly at Lysaker, during the spring of 2015. The scope of the thesis was developed in collaboration with Lundin Norway AS, which also contributed with data and assistance throughout the execution of the work. Trym Elseth worked as the thesis supervisor from Lundin Norway AS, while Associate Professor Pål Skalle was the thesis supervisor from NTNU.

I would like to express my sincere gratitude for all conceptual, technical and motivational input received during the work on present thesis. So many skilled and committed people have contributed with their expertise and time, and without them, the realization of present thesis would not have been possible. I would like to thank Lundin Norway AS for giving me the opportunity to work with data and issues they are currently facing and for helping me develop an interesting, relevant and educational topic for present thesis. Special thanks goes to Trym Elseth for all guidance and discussions. I am truly grateful to all involved Lundin Norway AS employees, who have impressed me with their enthusiasm towards present thesis and have supported me whenever needed. The guidance and feedback received from my supervisor Pål Skalle was essential for the development and completion of present thesis, and for this, I am truly grateful. I would also like to express my gratitude towards fellow students, friends and my family for help and support during the work on present thesis.

Abstract

The high drilling cost of today's oil and gas industry makes drilling optimization highly desirable. Lost time during drilling caused by unforeseen challenges is common, and increases well cost. The elimination of such challenges enables a large cost-saving potential.

Several drilling challenges are associated with interaction with hard formations. Large variations in mechanical properties within a formation, often caused by harder stringers or boulders, can cause drilling challenges like buckling, dogleg generation, washouts and vibration. These challenges are all associated with extensive bit wear, BHA failure and slow penetration rate, resulting in lost time.

The appraisal drilling campaign on the Lundin Norway AS operated field Edvard Grieg have shown that large granitic boulders within conglomerate formations cause extensive bit wear, resulting in slow penetration rate and lost time. A data-agent developed to detect these conglomerate formations have been proposed in present master thesis.

The data-agent imports the relevant drilling parameters weight on bit (WOB), rotary speed (RPM) and penetration rate (ROP) from acquired drilling data. A simplified version of the mathematical model of penetration rate, proposed by Bourgoyne and Young (1986), have been used to calculate drillability. Further, formation hardness, the inverse of drillability, was calculated and displayed as a plot of formation hardness against depth. Some functional relations of the original penetration rate model were neglected, assuming they had negligible effect on the penetration rate over short spans. Both an average value of empirical exponents and the use of specific exponents for soft and hard formations, determined continuously by a moving average calculation, have been used in the data-agent.

Results from the data-agent showed few tendencies in detecting conglomerate formations between six Edvard Grieg wells. The expected difference in formation hardness between sandstone and conglomerate formations was not proven. The results concluded that the model was not able to detect conglomerate formations.

Sammendrag

Dagens høye borekostnader i olje- og gassindustrien fører til økt interesse for boreoptimalisering. Nedetid under boreoperasjoner forårsaket av uforutsette boreutfordringer er vanlig, og bidrar til en dramatisk økning av borekostnader. Å eliminere slike boreutfordringer muliggjør derfor et stort potensiale for kostbesparelse.

Flere boreutfordringer assosieres med interaksjon med harde formasjoner. Store variasjoner i mekaniske parametere innenfor samme formasjon kan forårsake boreutfordringer som buckling, doglegs, utvasking og vibrasjon. Alle de nevnte boreutfordringene er assosiert med slitasje av borekronen, BHA-svikt og lav penetrasjonsrate, som resulterer i nedetid.

Boring av avgrensingsbrønner på Edvard Grieg feltet, operert av Lundin Norway AS, har vist at store granitt-knoller i konglomeratformasjoner har forårsaket omfattende slitasje på borekrone, resulteret i lav penetrasjonsrate og bidratt til uforutsett nedetid. En data-agent utviklet for å oppdage disse harde konglomeratformasjonene har blitt presentert i gjeldene masteroppgave.

Data-agenten importerer de relevante boreparameterne vekt-på-bit (WOB), rotasjonshastighet (RPM) og penetrasjonsrate (ROP) fra anskaffet boredata. En forenklet versjon av den matematiske modellen for penetrasjonsrate foreslått av Bourgoyne og Young (1986), har blitt brukt til å kalkulere borbarhet. Videre ble formasjonshardhet, den inverse av borbarhet, kalkulert og fremstilt grafisk som et plot av formasjonshardhet mot dyp. Noen underfunksjoner fra den originale penetrasjonsratemodellen har blitt neglisjert grunnet antagelser om at disse har en neglisjerbar effekt over korte intervaller. Ulike relevante eksponentverdier har blitt utprøvd, med hovedbruk av gjennomsnittsverdier.

Resultatene fra data-agenten viste få tendenser til å oppdage konglomerateformasjoner for seks Edvard Grieg-brønner. Den antatte forskjellen i formasjonshardhet mellom sandstein og konglomerat ble ikke påvist. Modellen brukt i gjeldene masteroppgave viste seg ikke egnet til å oppdage konglomeratformasjoner.

Table of Content

Acknowledgement.....	i
Abstract	iii
Sammendrag.....	v
Table of Content.....	vii
List of Figures	ix
List of Tables.....	xiii
1 Introduction	2
2 Relevant Published Knowledge	4
2.1 Generation of hard formations	4
2.2 Drilling Problems Caused by Hard Formations	8
2.2.1 Equipment Failure	8
2.2.2 Borehole Damage	8
2.2.3 Vibrational Problems Related to Hard Formations.....	10
2.3 Previous Attempts on Revealing Hard Formations through Real-Time Drilling Data Acquisition.....	12
2.4 Formation Hardness and Drillability.....	17
2.5 Calculating Formation Hardness through Mathematical Model of Penetration Rate	21
2.5.1 Warren’s Drilling Rate Model.....	22
2.5.2 Bourgoyne and Young’s Drilling Model.....	24
3 Model of Hardness in Edvard Grieg Conglomerates	28
3.1 The Edvard Grieg Field	28
3.2 Physical Understanding of Drilling Challenges Associated with the Edvard Grieg Conglomerates	30
3.3 Mathematical Model of Formation Hardness	36
3.3.1 Simplification of Model.....	36
3.3.2 Determination of exponents.....	38
4 Testing of Model	40
4.1 Acquired Real-Time Drilling Data	40
4.2 Analysis of Available Data	42
4.3 The Formation Hardness Detecting Data-Agent.....	43

5	Results	48
5.1	Results of Running the Hardness Detection Data-Agent.....	48
5.2	Comparison of Data-Agent Results with Facies Logs	57
5.3	Summary of the most helpful observations from the data-agent	61
6	Discussion	62
6.1	Applicability of Results	62
6.2	Quality of Data.....	64
6.3	Quality of Model.....	65
6.4	Future work.....	66
7	Conclusion.....	68
8	Nomenclature	70
9	Bibliography.....	72
	Appendix A – IADC Dull Bit Grading	78
	Appendix B - Core Drilling Information Table for Well A-D.....	80
	Appendix C – The MATLAB Program.....	86

List of Figures

Figure 2-1: Principle sketch of stress versus deformation in a uniaxial compression test (Fjaer et al. 2008)..... 6

Figure 2-2: Washout caused by a buckled drill string due to excessive weight on bit (Solberg 2012)..... 9

Figure 2-3: Key seats induced by hole deviation and variation of formation hardness (Schlumberger 2014b)..... 10

Figure 2-4: Types of vibration and associated drilling challenges (Schlumberger 2010)..... 11

Figure 2-5: Modified schematic of optimum drilling parameters to avoid drilling challenges associated with vibration (Wu et al. 2010)..... 12

Figure 2-6: Artistic illustration of a high local dogleg developed at the surface of a calcite cemented stringer (Hood et al. 2003). 14

Figure 2-7: Modified figure from the Haynesville shale gas play. rilling interval is showing the correlation between surface (center) and downhole measured drilling speed (right). Stable values of surface speed while downhole speed is oscillating (circled), indicates stick slip (Dykstra, Schneider, and Mota 2011). 16

Figure 3-1: The four different reservoir types of the Edvard Grieg field.1- Sandstone, 2- Conglomeratic sandstone, 3-Conglomerate, 4-Weathered and fractured basement (LundinNorwayAS 2014)..... 29

Figure 3-2: General zone classification of formations inside and surrounding the Eedvard Grieg reservoir..... 31

Figure 3-3: Determination of UCS from triaxial tests from two different Edvard Grieg conglomerates (Hilgedick et al. 2012) 32

Figure 3-4: Triaxial test sample from weak matrix conglomerate from the Edvard Grieg field (Hilgedick et al. 2012)..... 33

Figure 3-5: Ringed out bit and one nozzle missing after drilling through Edvard Grieg conglomerate (Hellvik et al. 2012)..... 35

Figure 4-1: Geographic location of Well A-F, drilled on the Edvard Grieg Field (Wenum 2015). 41

Figure 4-2: Data process flow of formation hardness detection data-agent..... 44

Figure 5-1: Formation hardness log for Well A, displayed with four different settings of the moving average MATLAB smoothing function. Average exponent values have been used to calculate the formation hardness. From the left: No smoothing have been used, a moving average over the last 3 acquired data points have been used, moving average over the last 5 points and moving average over the last 10 points. 49

Figure 5-2: Well A. ROP, RPM, WOB and calculated Formation Hardness plotted against depth of cored 8 ½” interval. Average exponent values ($a_5 = 1.3$ and $a_6 = 0.7$) have been used to calculate the formation hardness. 49

Figure 5-3: Well B. ROP, RPM, WOB and calculated Formation Hardness plotted against depth of cored 8 ½” interval. Average exponent values ($a_5 = 1.3$ and $a_6 = 0.7$) have been used to calculate the formation hardness. 50

Figure 5-4: Well C. ROP, RPM, WOB and calculated Formation Hardness plotted against depth of cored 8 ½” interval. Average exponent values ($a_5 = 1.3$ and $a_6 = 0.7$) have been used to calculate the formation hardness. 51

Figure 5-5: Well D. ROP, RPM, WOB and calculated Formation Hardness plotted against depth of cored 8 ½” interval. Average exponent values ($a_5 = 1.3$ and $a_6 = 0.7$) have been used to calculate the formation hardness. 52

Figure 5-6: Well E. ROP, RPM, WOB and calculated Formation Hardness plotted against depth of cored 8 ½” interval. Average exponent values ($a_5 = 1.3$ and $a_6 = 0.7$) have been used to calculate the formation hardness. 53

Figure 5-7: Well F. ROP, RPM, WOB and calculated Formation Hardness plotted against depth of cored 8 ½” interval. Average exponent values ($a_5 = 1.3$ and $a_6 = 0.7$) have been used to calculate the formation hardness. 54

Figure 5-8: Formation hardness in logarithmic view plotted against depth for all wells, Well A-F. Average exponent values ($a_5 = 1.3$ and $a_6 = 0.7$) have been used to calculate the formation hardness. 55

Figure 5-9: Formation hardness for Well A calculated with static exponent values and automatic changing exponent values. The red line shows formation hardness calculated by using the average exponent values ($a_5 = 1.3$ and $a_6 = 0.7$). The blue line shows formation hardness calculated by using a moving average, times a threshold value, to determine whether soft formation exponent values ($a_5 = 1.1$ and $a_6 = 0.8$) or hard formation exponent values ($a_5 = 1.5$ and $a_6 = 0.6$) should be used to calculate the formation hardness. 56

Figure 5-10: Formation Hardness plotted against depth compared to the local facies log for Wells A, B and C. Average exponent values ($a_5 = 1.3$ and $a_6 = 0.7$) have been used during calculation of formation hardness. Table 5-1 explains the color scaling of the facies logs..... 57

Figure 5-11: Formation Hardness plotted against depth compared to the local facies log for Wells D, E and F. Average exponent values ($a_5 = 1.3$ and $a_6 = 0.7$) have been used during calculation of formation hardness. Table 5-1 explains the color scaling of the facies logs..... 58

Figure 5-12: Formation Hardness compared to the local facies log for Well A. The formation hardness was calculated with average exponent values (red) and the moving average data agent determining whether to use soft ($a_5 = 1.1$ and $a_6 = 0.8$) or hard ($a_5 = 1.5$ and $a_6 = 0.6$) formation exponent values (blue). 61

List of Tables

Table 2-1: Field test for compressive strength of rocks (Standford 2014)..... 7

Table 2-2: Unconfined compressive strength of different rock types (Standford 2014). 7

Table 2-3: Numeric results after Task Force initiative for drilling optimization in calcitic stringers within the Troll Field (Fiksdal, Rayton, and Djerfi 2000). 14

Table 2-4: Example parameter road map for the intermediate hole section of the Haynesville shale gas play (Dykstra, Schneider, and Mota 2011)..... 17

Table 3-1: Stress results from triaxial tests of two different conglomerate samples from the Edvard Greig field. The tests were run on different core samples at 2, 5, and 10 MPa confining stress (Hellvik et al. 2012)..... 32

Table 3-2: Dull Bit Grading after drilling in conglomerate formations on the Edvard Grieg Field. (Bialon et al. 2010, Huse and Magnussen 2008, Johnsrud et al. 2009, Skuncke 2014) 33

Table 4-1: Depths of coring intervals for Well A-E..... 43

Table 4-2: Values for bit weight and rotary speed exponents used in the data-agent..... 45

Table 5-1: Description of color scaling of facies logs for Wells A-F. 57

1 Introduction

Operational lost-time incidents, caused by unexpected drilling challenges, contribute to a substantial increase in well cost during drilling operations. The saving potential from mitigating such challenges, when daily drilling cost exceed 1MNOK per day in the Norwegian North Sea, is significant. Therefore, it is of interest to the oil and gas industry to optimize drilling within challenging formations.

Hard formation characteristics, such as boulders and stringers, cause large variations in mechanical properties within a formation. A sudden change in hardness and rock strength can lead to a decrease in penetration rate, which in turn induces a weight on bit increase from the driller. Excess weight on bit in hard formations can lead to drill string buckling, dogleg generation and washouts. Vibration of the drill string induced by rough drilling in hard formations causes severe drilling challenges such as stick slip, bit bounce and bit whirl. The drilling challenges mentioned are all associated with decreasing penetration rate, wellbore damage, equipment failure and general lost time during operation.

Conglomerate formations containing hard granitic boulders within the Lundin Norway AS operated Edvard Grieg Field have proved severe drilling challenges. Low penetration rate and extensive bit wear are challenges faced when drilling the conglomerate. Optimization of penetration rate within the conglomerate, with respect to preservation of bit properties, would help decrease non-productive time, and consequently reduce drilling cost for the current field development.

Present thesis examines the generation of different hard formations and investigates the drilling challenges met when drilling these formations. A literature study presents published knowledge on how to optimize drilling within such formations. The work done in present thesis attempts to detect the conglomerate formations of the Edvard Grieg field through formation hardness and a modified version of Bourgoyne and Young's (1986) mathematical model of penetration rate. A data-agent calculating the formation hardness through acquired drilling data is proposed.

Finally, the results obtained from the data-agent are compared with the local geology at the respective well.

The goal of present thesis is to eliminate non-productive time associated with drilling the Edvard Grieg conglomerates. The step taken in present thesis towards reaching this goal is to develop a data-agent that will detect the conglomerates. Early detection of the challenging conglomerate formations will enable the driller to instantaneous alter drilling parameters, to obtain the most efficient penetration rate with respect to drillability and bit wear.

2 Relevant Published Knowledge

Hard formations is a major contributor to rough drilling conditions. Bit wear, formation damage and vibrations of the drill string causing bottom hole assembly (BHA) failure, bit bounce, stick-slip and bit whirl are all drilling complications associated with harder formations. The geological reasons for some formations being harder than others can be many, including cementations, crystallization, metamorphosis or simply the presence of boulders. Many different oil and service companies have spent an extensive amount of resources trying to optimize drilling operations in such hard and troublesome formations. Present chapter will examine different causes of generation of especially hard geological formations, and account for different drilling problems associated with them. Further, the chapter presents existing knowledge on revealing hard formations through real-time drilling data. The concept of drillability and formation hardness will be presented, before ending respectively with the presentation of mathematical models of penetration rate used to detect formation hardness. This chapter is an extended version of the specialization project by Nilsen (2014).

2.1 Generation of hard formations

Hard formations are often associated with igneous or metamorphic rocks, but in the oil and gas industry, sedimentary rocks that have gone through cementation and/or compaction can also be classified as hard formations. Present thesis will focus on hard, sedimentary rocks.

Sedimentary rocks are generated through sediment deposition, where the sediments originate from weathered rocks, biogenic activity or precipitation from solutions. Clastic, sedimentary rocks such as conglomerates, sandstones, siltstones and clay, form as the sediments of weathered rocks accumulate and harden through compaction and cementation. Biogenic sedimentary rocks, like limestone, form due to organic activity, as in coral reefs. Precipitated sedimentary rocks, as halite and gypsum, can form due to evaporation of seawater. Typical minerals in sedimentary rocks are quartz, feldspar, calcite, dolomite, evaporite groups and clay groups (Schlumberger 2014c). The most important cause of some sedimentary rocks being

harder than others is mainly due to the degree of cementation and the cementation material of the rock.

The thought of a formation being homogenous seems convenient during the drilling process. That would make the prediction of tool and bit damage easier, and consequently help select the best-suited tools prior to the operation. In practice however, variation of geological properties between different, or inside the same formations, are common. Geological phenomenon that causes such variation within the same formation, as boulders and stringers, are often smaller and therefore harder to predict prior to the drilling operations, and can cause unexpected drilling difficulties.

Conglomerate is an example of a formation where the mechanical properties changes rapidly within the formation. The clastic sedimentary rock contains large, rounded clasts, and the space between the clasts is generally filled with smaller particles, like sandstone or siltstone, and/or chemical cement that binds the rock together (King 2015). Conglomerate can have a varying degree of sorting, from small pebbles (> 4 mm), cobbles (> 64 mm) to large boulders (> 256 mm) (Alden 2015).

Pieces of rock larger than 25 cm are defined as boulders. The transportation of the boulders from their origin occurs as high-energy transportation processes involving ice or water, erodes rock formations and moves the boulders to a low-energy area, where they are deposited (Thefreedictionary 2003a). A formation comprised of boulders causes a drilling environment with high variations in drilling parameters between the matrix and the framework, which complicates the drilling operation.

Another geological phenomenon that creates heterogeneous formations are stringers, which are thin and hard, discontinuous mineral veins or rock layers up to 3 m thick (Thefreedictionary 2003b) (personal communication; Skalle, 2015). Stringers are generated through precipitation, calcite concretization or evenly cemented layers within the sedimentary formations.

A way to distinguish the difference in strength between different rock types is to define the rock by the unconfined compressive strength (UCS) (also called uniaxial compressive strength). UCS is the maximum allowed stress applied to a rock sample, before permanent deformation that inhibits the rock ability to support load occurs. The different stress parameters are found through a uniaxial test, and the results as increasing stress is applied to the sample, are shown in Figure 2-1. The elastic region of the graph represents the applied stress interval where the sample deforms, but returns to its original strength once the stress is reduced. The ductile region is where permanent damage to the sample occurs, but the rock will still be able to support load. In the brittle region, the sample's ability to withstand the applied stress decreases rapidly. In practice, the ductile region is often very small (Fjaer et al. 2008).

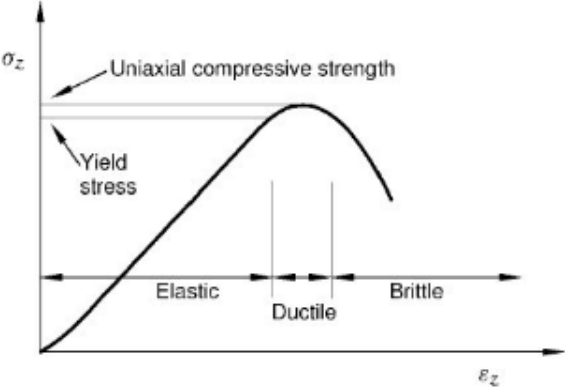


Figure 2-1: Principle sketch of stress versus deformation in a uniaxial compression test (Fjaer et al. 2008).

Table 2-1 describes a rock type's strength, or hardness, while the typical UCS values for different common rock types are listed in Table 2-2.

Table 2-1: Field test for compressive strength of rocks (Standford 2014).

Term	Diagnostic features	Unconfined compressive strength
Weak Rock	Crumbles with blows of pick end of hammer	1.25 -5 MPa
Moderately weak rock	Too hard to cut by hand	5-12.5 MPa
Moderately strong rock	5 mm indentations with hammer pick end	12.5-50 MPa
Strong Rock	Hand specimen can be broken with single blow	50-100 MPa
Very strong rock	Very hard rock, requires repeated hammer blows	>100 MPa

Table 2-2: Unconfined compressive strength of different rock types (Standford 2014).

Rock type	Unconfined compressive strength
Granite	100-250 MPa
Basalt	100-300 MPa
Quartzite	150-300 MPa
Sandstone	20-170 MPa
Shale	5-100 MPa
Limestone	30-250 MPa
Marble	35-60 MPa
Slate	100-200 MPa
Quartzite	150-300 MPa

2.2 Drilling Problems Caused by Hard Formations

As stated previously, hard formations may cause difficult drilling conditions. Decreasing penetration rate, dogleg generation, equipment failure and problems associated with excessive vibration downhole, are all examples of known problems connected to hard formations. Wear or damage to the bit or BHA may cause unplanned trips out of hole. Borehole damage like doglegs may cause the drill string to get stuck. Additionally, vibrational consequences as bit bounce, stick slip, bit whirl and bending may cause a combination of several challenges. The drilling problems listed below are selected examples, not an effective list of all, associated with unexpected non-productive time (NPT), and are to be avoided for a cost efficient, optimized drilling operation.

2.2.1 Equipment Failure

When drilling into a hard formation, extensive bit wear is often experienced. This may have to do with the lack of knowledge regarding the formation drilled. This lack of knowledge can lead to the wrong bit selection, rather than choosing a bit customized for hard formations. Wearing of the bit teeth will then occur and penetration rate decrease. As damaged bits need replacement, unanticipated bit runs have to be conducted, to an extra cost.

A consequence of low ROP is for the driller to add extra weight to the bit. If the penetration rate is not responding to this weight gain, the torque of the drill sting will increase. If the torque overrides the design criteria of the components in the drill string, damage or complete tool failure may occur (Solberg 2012).

2.2.2 Borehole Damage

Another consequence of the additional weight on bit mentioned in section 2.2.1 is buckling of the drill string. As added weight on bit in a straight hole-section reaches a critical point, the drill sting will no longer maintain its verticality. Due to the vertical compressional forces, the drill string will start buckling (Lubinski 1950, Bourgoyne et al. 1986). The buckling movement

will make the drill string collide with the surrounding borehole wall. When a soft formation is overlaying a hard formation, this buckling movement will cause a washout, that is, an enlargement of the borehole wall (Schlumberger 2014d). An illustration of the phenomenon is shown in Figure 2-2. A washout of this sort may cause the drill sting to stick at the ledges between the soft and hard formation interfaces, during tripping in and tripping out.

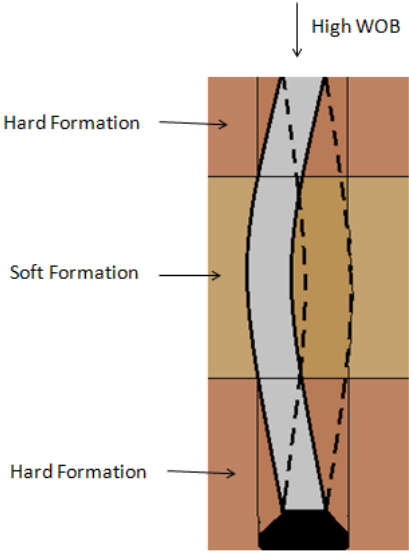


Figure 2-2: Washout caused by a buckled drill string due to excessive weight on bit (Solberg 2012).

When drilling from a soft formation into a hard formation, the unintended generation of doglegs may happen. Doglegs are defined as sections of the borehole changing direction faster than anticipated or desired. There are several problems associated with doglegs. If the hole deviates from the planned trajectory, one can experience problems running in hole with the casing, or the casing may wear extensively. Problems running a relatively stiff BHA through the dogleg section of the hole may also occur. Unwanted doglegs increases the overall friction in the well, and increases the chances of the drill string getting stuck or not reaching planned depth. (Schlumberger 2014a).

In a dogleg section of a well, repeated abrasion by the drill sting on the borehole wall at a specific point may create a small-diameter channel worn into the wellbore wall, called a key seat. A key seat can also generate if a hard formation ledge is left between softer formations that enlarge over time, as shown in Figure 2-3. This can result in the drill string getting stuck when pulling out of hole, and larger-diameter portions of the drill string, like drill collars,

stabilizers and other BHA components try to pass through the smaller-diameter key seat (Schlumberger 2014b).

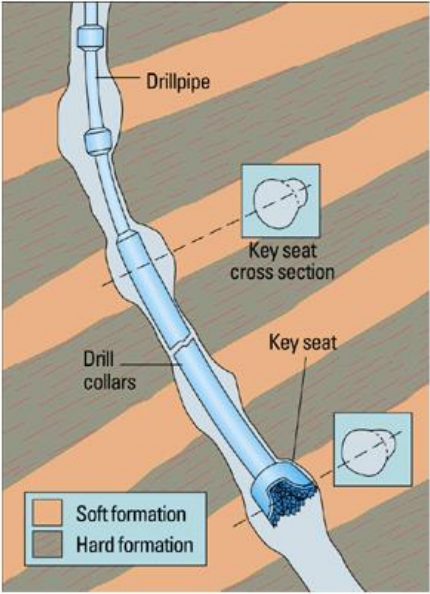


Figure 2-3: Key seats induced by hole deviation and variation of formation hardness (Schlumberger 2014b).

2.2.3 Vibrational Problems Related to Hard Formations

As the drill bit enters a hard formation, vibration created from the impact start to generate, and propagates through the bit, the BHA and the drills string. Effective vibration is said to have a large influence on the penetration rate (personal communication; Skalle, 2015). Experiences have shown reducing high vibration levels in the drill string, generated from drilling through hard rock, can decrease non-productive time and contribute to more profitable endeavor (Santos et al. 2000). There are three different types of drill string vibration, all associated with different drilling problems. The Schlumberger brochure *Drillstring Vibration and Vibration Modelling* (2010) and Figure 2-4 are used further to describe the different vibrational types and their associated drilling complications.

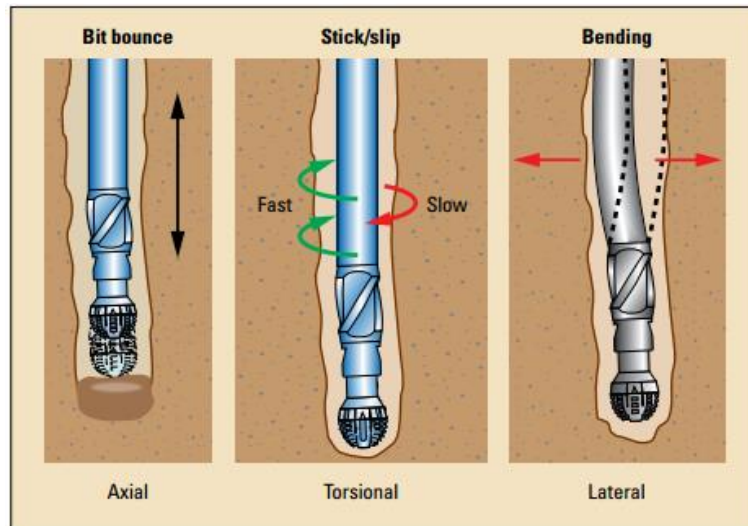


Figure 2-4: Types of vibration and associated drilling challenges (Schlumberger 2010).

Axial vibration is vibration in the vertical direction. This movement can cause bit bounce. The continuous impact between the bit and the hard formation can damage the cutters and bearing of the bit, which in turn leads to extra bit runs.

Torsional vibration is angular vibration of the drill string. This causes irregular downhole rotation, which in its most severe form, causes stick slip phenomenon. Stick slip occurs when the bit becomes stuck in the hard formation over a period. This causes torque to build up in the drill string. Subsequently, the bit slips and the acceleration of the drill bit increases rapidly. The torsional fluctuations will fatigue drill collar connections and damage the drill bit.

Lateral vibration is vibration in the horizontal plane. The interaction between the BHA and the drill string contact points can drive the drill string into backward whirl. This phenomenon creates high-frequency large-magnitude bending momentum fluctuations, and is the most severe form of vibration. The consequences of backward whirl are connection and component wear, and in a worst-case scenario equipment failure.

The three types of drill string vibration occur during rotary drilling and can induce each other. For example, once axial bit vibrations occur, this motion generates lateral vibrations in the BHA.

Wu et al. (2010) stated that vibrational induced drilling challenges, such as stick slip and whirl, significantly limits the drilling performance. Vibrations can cause equipment failure and increase non-productive time driving up field development cost. The driller’s dilemma emerges when increasing WOB induces stick slip, increasing RPM induces whirl and combining high WOB and low RPM induces bit bounce (Wu et al. 2010) (personal communication; Zhao, 2015). Therefore, knowing the optimum zone of drilling parameters is desirable during drilling operations. See Figure 2-5.

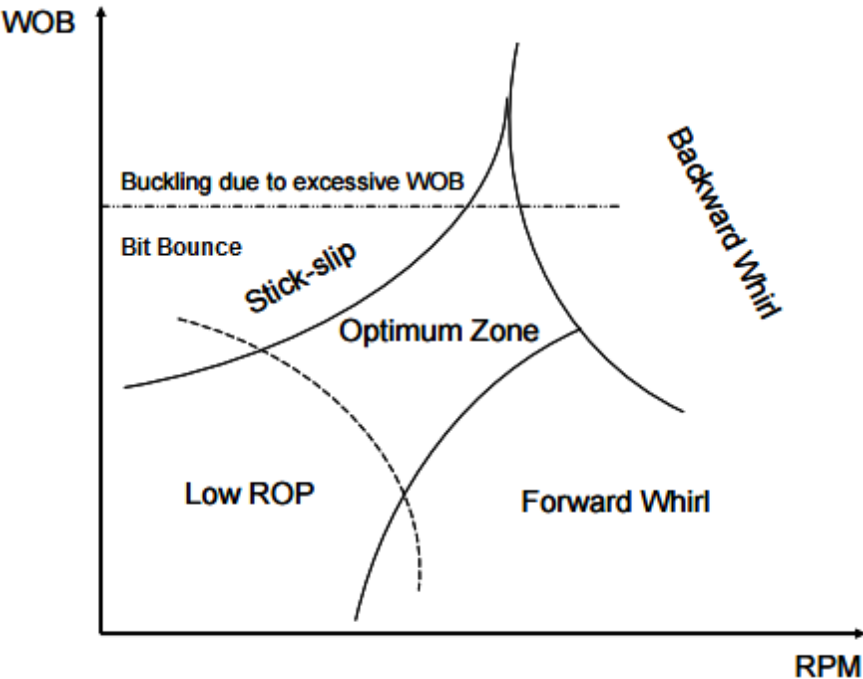


Figure 2-5: Modified schematic of optimum drilling parameters to avoid drilling challenges associated with vibration (Wu et al. 2010).

2.3 Previous Attempts on Revealing Hard Formations through Real-Time Drilling Data Acquisition

As shown in the previous subchapters, hard formations are challenging drilling environments. Many oil companies, service companies and research institutions have investigated how to manage these formations during drilling, to lower drilling costs. Research on how to use different specialized tools to better penetrate the hard formations has been conducted thoroughly. To increase the rate of penetration in hard rock, promising technologies like

thrusters, hydraulic hammers, jet-assisted drilling systems and mini disc bits have gone through field tests with varying results. Some of which proved to increase the rate of penetration (Santos et al. 2000). This thesis however, will investigate the revealing of hard formations through real-time drilling data (RTDD) during drilling operations. As the drill bit intercepts the hard formations, changes in drilling parameters will occur. These parameters can in turn be adjusted by the driller to optimize the drilling conditions in the given, hard formation.

The Sognefjord reservoir of the Troll field in the Norwegian North Sea consists of loose sands, subdivided into clean and micaceous units and local hard calcareous cemented zones. The horizontal reservoir section have been drilled with rotary steerable tools (RSS). The hard calcite stringers have proved large variations in penetration rate, short bit runs due to worn bits and unwanted influence on the BHA behavior. This made corrections with respect to drilling optimization necessary. Fiksdal et al. (2000) gathered a task force of Norsk Hydro and service company representatives to optimize drilling operations on the Troll field.

The calcite-cemented stringers were not uniformly distributed in the sandstone reservoir. The uncertainty on where and when the stringers would appear, made mapping and prediction of the stringers an area of potential improvement for the research task force. During the well planning phase prior to the task force initiative, the mapping of the calcite stringers was performed through acoustic impedance derived from seismic data, and evaluated spatially using advanced 3D visualization techniques. This method was however not reliable on calcite stringers of smaller lateral extent. Therefore, the extensive downhole vibrations measured in real-time as the bit drilled into the calcites, were used to alert the driller of stringer interaction with the bit. This allowed the driller to alter drilling parameters to optimize the drilling operation when interacting with the hard stringers. After several simulated test runs in calcite, a drilling parameter guideline was developed for further development of the Troll field. The guidelines included recommendations on WOB, RPM, parameters while entering/exiting the calcite zones and parameters while drilling in calcite zones. Personnel involved in the drilling operations received comprehensive training on how to optimize the drilling using these guidelines. Specific focus was given on parameter alteration when drilling into the calcite. For example, in general the RPM was reduced before WOB gradually was increased to a level where drilling progress into the calcite stringers could be made.

The drilling parameter guidelines, combined with drill bit and BHA optimization, managed to increase drilling performance of well sections where the average percentage of calcitic sandstone was above 7%. Numeric results are listed in Table 2-3 (Fiksdal, Rayton, and Djerfi 2000).

Table 2-3: Numeric results after Task Force initiative for drilling optimization in calcitic stringers within the Troll Field (Fiksdal, Rayton, and Djerfi 2000).

	Prior to task force initiation	After task force initiatives
Average run length	388	641
Average ROP	10.7	20.5
Number of bit runs	10.4	4.6

Another problem associated with the calcite stringers within the Troll field reservoir is high local doglegs (HLD), induced when entering and exiting the stringers during drilling. Depending on the dip angle and the orientation of calcite stringer surfaces, the bit can be forced aside into the more drillable loose sands surrounding the stringers, as seen in Figure 2-6. Hood et al. (2003) initiated a study on how real-time BHA bending information could reduce the risk of creating these high local doglegs.



Figure 2-6: Artistic illustration of a high local dogleg developed at the surface of a calcite cemented stringer (Hood et al. 2003).

A downhole-dynamics tool was positioned above the rotary steerable system in the BHA. This tool processed high rate measurements of 14 drilling process sensors, and further diagnosed the occurrence and severity of various drilling-dynamics phenomena. In this case, the relevant data collected from the tool was its ability to measure bending moment in the BHA, generated by side forces at the bit and at other wall contact points of the BHA. Previous downhole tools used to measure bending moment would work in vertical sections of the well, as it measured adequately inclinational changes of the BHA. Measurements of the azimuthal changes were however, not working adequately. The new downhole-dynamics tool delivered these measurements in the horizontal reservoir section, and they were processed real-time at surface. Once a dogleg in the well path was observed at surface, the driller and the directional driller changed the drilling parameters, and the RSS was steered less aggressively back to the target vertical depth. The implementation of the real-time downhole bending moment measurements during drilling have contributed to improved understanding of the downhole environment, and reduced dogleg related failures. This implies decreased average number of runs required to drill the Troll reservoir section. The reduction of HLD has also improved the overall hole quality, reduced torque losses, drill string wear and problems during completion (Hood et al. 2003).

Dykstra, Schneider, and Mota (2011) summarized a *Drilling Efficiency Optimization* (DEO) project of the Haynesville shale gas play in North Louisiana, US. The hard and abrasive Hosston sandstone-shale sequence and hard Knowles limestone in the intermediate section of the overburden were known for causing bit and drill string vibrations. This lead to short bit runs with low penetration rate due to stick slip and bit whirl, as well as unacceptably high cost per foot (cpf). One of the focus points of the DEO program was actively management of drilling parameters. An example of this was comparing surface and downhole rotational speed to recognize stick slip occurrence. The average surface speed could read 100 RPM, while downhole speeds oscillated between 0 and 300 RPM, indicating severe stick slip as indicated in Figure 2-7.

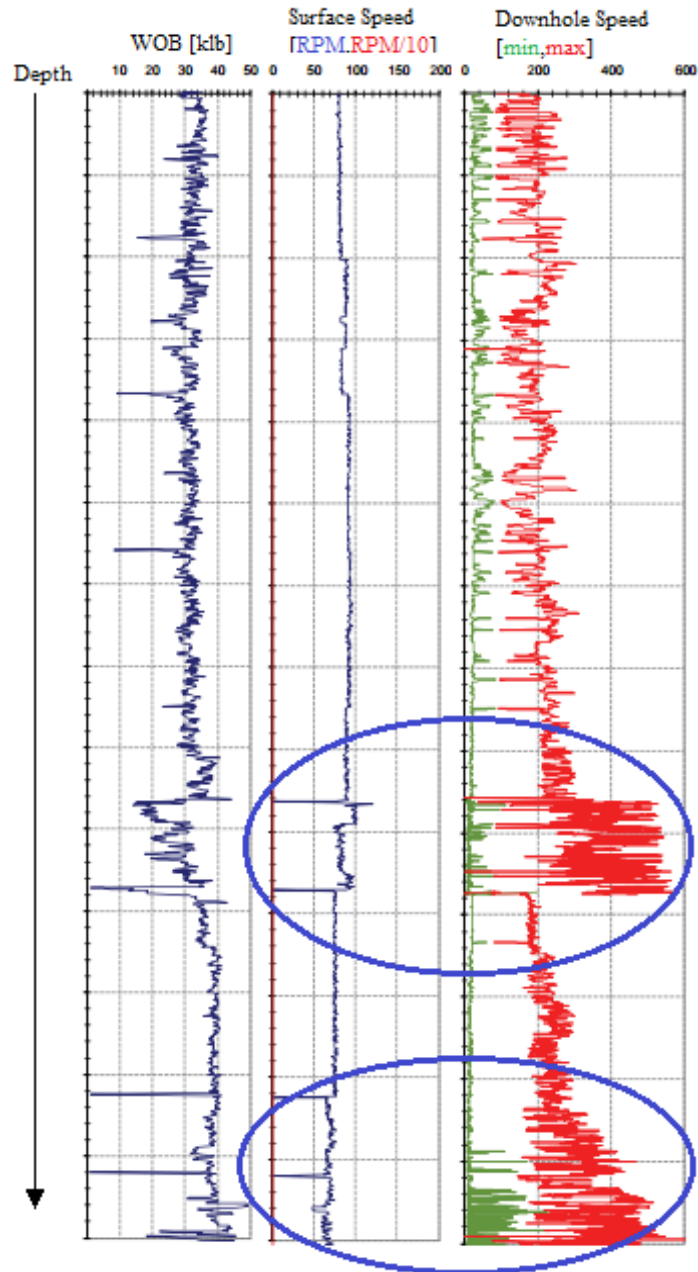


Figure 2-7: Modified figure from the Haynesville shale gas play. rilling interval is showing the correlation between surface (center) and downhole measured drilling speed (right). Stable values of surface speed while downhole speed is oscillating (circled), indicates stick slip (Dykstra, Schneider, and Mota 2011).

The active management of drilling parameters also included parameter “road maps”, with starting values of WOB and RPM for the driller in the formations of varying rock strength. See Table 2-4. Training of the drillers was also provided, to help the driller recognize when parameters needed to be changed, to mitigate vibration or other sources of inefficiency.

Table 2-4: Example parameter road map for the intermediate hole section of the Haynesville shale gas play (Dykstra, Schneider, and Mota 2011).

Interval [ft]	Weight on Bit [klb]	Bit Speed [RPM]	Flow Rate [gpm]	Comments
2,000-8,200	20-40	150-180	≥ 650	First bit of intermediate section Soft to medium strength formations
8,200-9,800	20-40	≤ 120 ≤ 100 preferred	≥ 650	Hosston – hard, abrasive Limit max combined surface + motor RPM
9,800-10,500	20-40	≤ 120 ≤ 100 preferred	≥ 650	Knowles – hard Limit max combined surface + motor RPM

Other real-time monitoring and intervention strategies used in the DEO program were the usage of an Stick-Slip Alarm (SSA) and mechanical specific energy (MSE). The SSA was based on the notion where the severity of torsional vibration was reflected in the magnitude of surface torque vibration over a given sampling period. The observation of MSE changes between rock strength and dull conditions of the bit has significantly reduced the “damage beyond repair” charges common in previous wells on the field. All of these real-time drilling data management strategies contributed to improve average ROP and run length in the hard formation intervals on the Haynesville field. The total combined efforts in the DEO program reduced cost per foot and days per thousand feet by over 50 % (Dykstra, Schneider, and Mota 2011).

2.4 Formation Hardness and Drillability

Mensa-Wilmot, Calhoun, and Perrin (1999), defined and quantified drillability as drilling difficulty, and established a differences between this and formation hardness. Overton (1973) defined drillability as the rate at which a given rock may be penetrated, while Somerton, Esfandiari, and Singhal (1969) defined drillability as the volume of rock drilled per unit of energy input.

From this, one can say that drillability is a quantitative way of displaying how easy or hard it is to drill a specific formation. The prediction of drillability will therefore give a good indication

of how hard the formation is (Solberg 2012). The relationship between the formation hardness and drillability, K , is shown in equation (2-1) below (personal communication; Skalle, 2015). This subchapter will take a closer look at some past studies of drillability.

$$\text{Formation Hardness} = \frac{1}{\text{Drillability}} = \frac{1}{K} \quad (2-1)$$

In order to optimize the choice of drill bits for different formations, Head (1951) developed a classification based upon the relative efficiency with which formations could be drilled. Such a classification was a step towards being able to optimize bit choice to what is considered a “soft formation bit” or a “hard formation bit”, based on what kind of formation they drill most efficiently. Head (1951) defined the efficiency with which a formation can be drilled to be dependent on the rate of penetration a bit can obtain within a formation. Therefore, the factors affecting rate of penetration must be studied and understood. Factors such as formation type, bit type, weight on bit, rotational speed, hydraulic action, hole size and efficiency of personnel and equipment, are being highlighted by Head (1951) to affect rate of penetration, where the geological formation being encountered is the only factor truly independent of control. Each formation encountered has its own properties that affect its resistance to penetration. Common formations to encounter during drilling are shale, salt, plastic clay, sand, gravel, limestone, dolomite and granite. Limited tests conducted to establish a relationship between hardness and drillability showed that the drillability of formations seemed more related to how hard crystals were bound together rather than to the hardness itself. However, the drillability classification developed proved to be consistent with actual drilling practices.

Somerton (1959) conducted laboratory tests to determine whether a model comparing the drill strength of rock would be applicable. Factors controlling rate of bit penetration was investigated conveniently by dimensional grouping through the model. See equation (2-2).

$$ROP = K * d_b * RPM * \left(\frac{WOB_e}{d_b^2 S} \right)^a \quad (2-2)$$

Here d_b is the bit diameter, WOB_e is the effective weight on bit, S is the rock strength parameter and a is exponent to be determined experimentally.

Somerton (1959) investigated the effects of rock strength and bit wear on drilling rates and drill cuttings were analyzed to determine the character of breakage. The rock strength parameter from equation (2-2) is the only parameter difficult to evaluate. From the investigation, it was found that ultimate compressive strength alone was not an adequate measure of rock drillability.

Somerton, Esfandiari, and Singhal (1969) took on several tests used to evaluate rock strength and rock drillability, as this value cannot be evaluated and determined by one single simple test. Somerton, Esfandiari, and Singhal (1969) investigated the correlation between the hardness tests and rock drillability tests. The drillability, defined as volume of rock drilled per unit of energy input, was determined from equation (2-3), where τ is torque. The hardness was determined from equation (2-2) presented by Somerton (1959):

$$K = \frac{ROP * \tau}{\tau * RPM} \quad (2-3)$$

The tests of Somerton, Esfandiari, and Singhal (1969) further investigated results from Gstalder and Raynal (1966) and confirmed that sonic velocity is a good indicator of rock drillability. A mineralogical factor must be considered in such correlations. The test was conducted on both limestone and sandstone. The work proved that a distinction had to be made between the two. Some of the results showed that limestone may have to be classified as “soft” or “hard” to obtain good correlations. The work also proved that rock drillability, K , seems to be a good correlating quantity in the range of medium weights on the bit. Low values of K were obtained at low weights, while the effects of high weights were not tested. Even though the value of drillability does vary with bit type, Somerton, Esfandiari, and Singhal (1969) found it likely that this quantity is a good indicator for the most efficient bit type for a given rock.

Yin (1986) established an equal probability correlation of bit type and drillability grades with experimental and statistical methods, for the variation of drillability with depth. He focused on creating a non-homogenous model, as past research often assumed the formation homogenous. Yin determined a conditional drillability grade K_d as the logarithm of the time used to drill down to a specific depth. This drillability grade was then used to create a parametric drilling rate equation. The equation proved to work effectively for bit selection and monitoring formation drillability while drilling, based on abundant drilling data from eight Chinese oil fields.

The work by Mensa-Wilmot, Calhoun, and Perrin (1999) presented formation drillability as a new bit performance evaluation parameter. The process of determining formation drillability combines different rock mechanical properties into one single dimensionless parameter that considers the magnitude of the different properties, length of the different formations and the percentage of the different lithologies in the formations encountered in a given hole size. This parameter enables quantification of drilling difficulty. In that way, limitations such as determining bit performance in an unknown field, and difficulties of comparing drillabilities between several wells in the same, or between different, fields are taken into account. The use of the term cpf is widely used within the industry to measure drilling optimization. Mensa-Wilmot, Calhoun, and Perrin (1999) argues however, that cpf does not take important factors such as rig type, well location, drilling program, operational environment and technological advancement into account. The formation drillability methodology presented by Mensa-Wilmot, Calhoun and Perrin is, when consistently used, said to improve operational efficiency, because of its ability to explain and predict drillabilities within the same, known field, as well as for new unknown fields.

In search for PDC bit performance optimization in harsh environments, Mensa-Wilmot and Fear (2001) examined the effects of formation hardness, abrasiveness and heterogeneity. They used the definition of formation drillability; characterized through drilling difficulty, to determine whether a formation was normal or harsh. As the drilling difficulty increases, the environments are seen as harsh. On operational efficiency, the penetration rate was seen as a unique performance qualifier, as it behaves differently in normal than in harsh conditions. In normal drilling conditions, the ROP has a direct influence on operation efficiency, but for harsh conditions, ROP has a more indirect influence. Here the ROP must be optimized together with other performance qualifiers such as stability and durability of the bit and BHA. The work of Mensa-Wilmot and Fear (2001) resulted in a new performance guideline for harsh drilling environments, which identifies the use of drilling parameter ranges that do not cause the bit or BHA to vibrate, as the most important operational requirement. The guidelines present optimal choices of PDC bit properties for drilling in hard, abrasive and heterogenous formations.

A method to determine drillability from sonic logs was attempted by Andrews et al. (2007). Correlations between sonic logs and the formation drillability were made for 10 different wells in North America. The drillability, known from rate of penetration models, was back calculated from the gamma ray log in conjunction with drilling parameters. The calculated drillability was correlated with sonic logs for different lithologies as defined by the gamma ray log. The different formation types present in the different wells clearly showed correlations for the normalized correlations between drillability and sonic logs. By the use of a program that created an Apparent Rock Strength Log (ARSL) from drilling data from a similar reference well, the study could create a drillability log for the planned well prior to the drilling operation. The ARSL log was then used to correlate with the back calculated drillability logs generated during operation. The study resulted in good correlation between the ARSL and the rock strength/drillability logs calculated from the sonic logs.

Many authors have proposed that there are correlations between drillability and formation hardness, as presented. This correlation, combined with real-time drilling data acquisition, will be further analyzed in present thesis.

2.5 Calculating Formation Hardness through Mathematical Model of Penetration Rate

Hareland et al. (2010) and others, state that one way of improving drilling efficiency, and to reduce cost, is to develop real time analysis tools that can predict and compare drilling performance. One way of modeling bit performance is to develop a model for optimal ROP. The penetration rate is one of the most important bit performance parameters, and optimizing ROP will increase efficiency and lower cost per foot drilled (Hareland et al. 2010) (Bourgoyne et al. 1986). Chapter 2.4 proved great correlation between drillability and penetration rate, and subsequently formation hardness. Therefore, mathematical models of rate of penetration will be examined in present subchapter.

The penetration rate is affected by many factors. The most important that have been identified and studied are bit type, formation characteristics, drilling fluid properties, bit operating

conditions (described as bit weight and rotary speed), bit tooth wear and bit hydraulics (Bourgouyne et al. 1986).

Several authors have presented mathematical models trying to predict penetration rate by combining the known variables that affect the rate of penetration. Although these are used today, some factors are difficult to predict, and there are some uncertainties related to the accuracy of the models. The most complete mathematical drilling models today include Bourgouyne and Young's model, Warren's model and later Warren's model modified by Hareland (Rahimzadeh et al. 2010). Present subchapter presents Warren's model and Bourgouyne and Young's model, but only one of the models will be used further in present thesis.

2.5.1 Warren's Drilling Rate Model

In 1987, Warren derived a model of the drilling process for tri-cone bits called perfect-cleaning model. Hareland later, in 1993, modified this. Warren states that under steady-state drilling conditions, the rate of cutting removal from the bit is equal to the rate at which new chips are formed. This implies that a combination, or either one, of the cutting-generation process and the cutting-removal process, manages the ROP (Rahimzadeh et al. 2010) (Hareland et al. 2010) (Hossain and Al-Majed 2015).

To develop a model of imperfect cleaning, Warren started by developing a perfect cleaning model.

$$ROP = \left(\frac{aS^2d_b^2}{RPM^bWOB^2} + \frac{c}{RPMd_b} \right)^{-1} \quad (2-4)$$

Here a, b and c are bit constants, to be determined experimentally.

In practice, ROP is often significantly inhibited by the rate of cutting removal from under the bit. To account for this, Warren used dimensional analysis to isolate a group of variables

consisting of the modified impact force and the mud properties. These variables were incorporated into the perfect cleaning model, to create the imperfect cleaning model.

$$ROP = \left(\frac{aS^2d_b^2}{RPM * WOB^2} + \frac{b}{RPM * d_b} + \frac{cd_b\gamma_f\mu}{F_{jm}} \right)^{-1} \quad (2-5)$$

Here γ_f is the fluid specific gravity, μ is the mud plastic velocity and the modified impact force can be calculated through equation (2-6).

$$F_{jm} = (1 - A_v^{-0.122})F_j \quad (2-6)$$

F_j is the jet impact force and A_v is the ratio of the jet velocity to the fluid return velocity. For three jets, A_v is calculated by equation (2-7).

$$A_v = \frac{v_n}{v_f} = \frac{0.15d_b^2}{3d_n^2} \quad (2-7)$$

Where v_n is the jet nozzle velocity, v_f is the return fluid velocity and d_n is the nozzle diameter.

To account for bit wear and chip hold down effects, Hareland (1993) modified Warren's model. To establish the best relationship for chip hold down, data from laboratory full-scale drill tests was used in which bottom-hole pressure varied and other conditions remained constant. The effect of bit wear on ROP was accounted for by a wear function. The modified model is given in equation (2-8).

$$ROP = W_f \left[f_c(P_e) \left(\frac{aS^2d_b^2}{RPM * WOB^2} + \frac{b}{RPM * d_b} \right) + \frac{cd_b\gamma_f\mu}{F_{jm}} \right]^{-1} \quad (2-8)$$

Where $f_c(P_e)$ is the chip hold down function and W_f is the wear function given by:

$$f_c(P_e) = c_c + a_c(P_e - 120)^{b_c} \quad (2-9)$$

$$W_f = 1 - \frac{\Delta BG}{8} \quad (2-10)$$

Here a_c , b_c and c_c are chip hold down permeability coefficients, P_e is the differential pressure and ΔBG is the change in bit tooth wear given in equation (2-11).

$$\Delta BG = W_c \sum_{i=1}^n WOB_i * RPM * Ar_{abr_i} * S_i \quad (2-11)$$

Ar_{abr} is the relative abrasiveness and S is the rock compressive strength as a function of pressure and lithology, shown in equation (2-12).

$$S = S_0(1 + a_s P_e^{b_s}) \quad (2-12)$$

Here a_s and b_s is the rock strength lithology coefficients.

All coefficients given in Warren's model needs to be determined to make use of the model. Coefficients a_c , b_c and c_c are depend on the formation permeability, a_s and b_s are lithology dependent, and coefficients a , b and c are bit coefficients that can be determined by plotting the dimensionless group ND/R vs $S^2 D^4 / W^2$. The wear coefficient W_c , can be determined by the dull condition of the bit.

Rahimzadeh et al. (2010) conclude that the accuracy of Warren's model is affected by the accuracy of the measured and evaluated rock strength. They also state that this penetration rate model is usually developed for a specific bit run and not for specified formations, such as Bourgoyne and Young's model.

2.5.2 Bourgoyne and Young's Drilling Model

Perhaps the most complete mathematical model of penetration rate for roller cone bits is the one proposed by Bourgoyne and Young (Bourgoyne et al. 1986). Later studies have shown that this model can be applicable for PDC bits as well (Personal communication; Skalle, 2015).

Bourgoyne and Young state that eight main functions of varying drilling parameters influence the rate of penetration. The main drilling variables incorporated into the model are formation strength, bit type, mud type, solids content, compaction, overbalance, bit weight, rotary speed, bit tooth wear and bit hydraulics. The model, containing the eight functions, is presented in equation (2-13).

$$ROP = (f_1)(f_2)(f_3)(f_4) \dots (f_8) \quad (2-13)$$

Function f_1 represents the drilling variables that are not considered in the other main functions. Conditions such as bit type, formation strength, mud type and solids content are examples of variables that should be considered. The value of f_1 vary with the strength of the formation being drilled, and is expressed in the same units as penetration rate. This function is often called the drillability of the formation. The drillability of various formations can be determined using drilling data obtained from previous wells drilled in the same area.

$$f_1 = e^{2.303a_1} = K \quad (2-14)$$

The functions f_2 and f_3 represent the effect of rock strength increase due to normal compaction and the effect of under-compaction experienced in abnormally pressured formations respectively.

$$f_2 = e^{2.303a_2(10000-D)} \quad (2-15)$$

$$f_3 = e^{2.303a_3D^{0.69}(g_p-9.0)} \quad (2-16)$$

Here D is the true vertical depth and g_p is the pore pressure gradient.

The effect of overbalance on penetration rate is modeled by equation f_4 .

$$f_4 = e^{2.303a_4D(g_p-\rho_c)} \quad (2-17)$$

Here ρ_c is the equivalent circulation density.

The functions f_5 and f_6 represent the effects of bit weight and rotary speed respectively.

$$f_5 = \left[\frac{\left(\frac{WOB}{d_b}\right) - \left(\frac{WOB}{d_b}\right)_t}{4 - \left(\frac{WOB}{d_b}\right)_t} \right]^{a_5} \quad (2-18)$$

$$f_6 = \left(\frac{RPM}{60}\right)^{a_6} \quad (2-19)$$

Where $(WOB/d_b)_t$ is the threshold bit weight per inch of bit diameter at which the bit begins to drill.

Function f_7 models the effect tooth wear on penetration rate.

$$f_7 = e^{-a_7 h} \quad (2-20)$$

Here h is the fractional tooth dullness.

Function f_8 represents the effect of bit hydraulics on penetration rate as shown in

$$f_8 = \left(\frac{F_j}{1000} \right)^{a_8} \quad (2-21)$$

The exponents a_1 to a_8 from equation (2-14) to (2-21) are constants based on local drilling conditions.

Bourgoyne and Young's model's ability to predict the penetration rate is primarily dependent on the method used to determine the constants a_1 to a_8 .

3 Model of Hardness in Edvard Grieg Conglomerates

As seen from the previous chapter, drilling in hard formations causes severe drilling challenges. Hard formations can lead to slow drilling progress and cause bit and tool wear, or failure. The result is often unplanned tripping operations and lost time, which increases drilling cost significantly.

The Lundin Norway AS operated field Edvard Grieg, currently under development, is an oil field that holds challenging conglomerate formations. The reservoir section of the field stretches into conglomeratic formations containing hard, granitic pebbles, cobbles and boulders. The drilling of these sections has proven to wear the bit, as well as significantly slow down the penetration rate. Present thesis will further examine the case of drilling challenges within and around the Edvard Grieg reservoir section. This chapter will present the Edvard Grieg field, explain the physical understanding of the drilling problems encountered during drilling operations, and present the mathematical model used in present thesis to reveal conglomerate formations from acquired drilling data.

3.1 The Edvard Grieg Field

Lundin Norway AS discovered the Edvard Grieg field in 2007, in block 16/1 of production license PL338. The field is located south on the Utsira High in the southern part of the North Sea, approximately 180 km west of Stavanger, Norway. The Edvard Grieg steel jacket platform, is currently under construction and the first oil is expected in October 2015 (LundinNorwayAS 2014, LundinPetroleumAS 2014).

The field comprises two discoveries, Luno and Tellus. Together they contain approximately 180 million recoverable barrels of oil equivalent. Other possible plays surrounding the Edvard Grieg field are expected to contribute to the total reserves. The Tellus discovery, located in the northern segment of the field, is the oldest reservoir of Edvard Grieg. It contains a 48 m oil column, in 440 million-year-old fractured and weathered basement rocks, in pressure communication with the Luno discovery. The Luno discovery ranges in age from 210 to 140

million years (Triassic, Jurassic and lower Cretaceous age), and consists of alluvial conglomerates, in parts with fluvial gravel and sands, and aeolian sands unconformably overlain by shallow marine sands. The reservoir is situated at a depth of approximately 1900 m below seabed, with the oil-water contact at 1939 m. The thickness of the oil column and the reservoir quality vary throughout the field (Hellvik et al. 2012, LundinNorwayAS 2014).

The reservoir quality varies from excellent to poor inside the reservoir, spanning from conglomerates to high quality sandstone and in parts porous basement (Tellus). The Jurassic and Triassic Luno reservoir depositional environment is alluvial fans, featuring short transported mixture of matrix supported polymodal conglomerates and sandstones, in parts transcending in to fluvial channel gravel and sand deposits, in parts as aeolian sand dune deposits. The conglomerate is comprised of a sandstone matrix with granite clasts, ranging from hard to very hard, in parts with rip-up clasts of clay. The clasts vary in size, angularity and distribution. The feldspar rich clasts have been eroded from the igneous basement highs surrounding the Luno basin (Hellvik et al. 2012, Hilgedick et al. 2012) (Personal communication; Aasheim, O., 2014). Figure 3-1 show the four different formation types that builds the Edvard Grieg reservoir.



Figure 3-1: The four different reservoir types of the Edvard Grieg field. 1- Sandstone, 2- Conglomeratic sandstone, 3- Conglomerate, 4- Weathered and fractured basement (LundinNorwayAS 2014).

After the Luno discovery in 2007, an extensive appraisal program has been conducted on the Edvard Grieg field. Nine wells have been drilled within the production license PL338. Fifteen new wells are planned for the on-going field development, twelve targeting the Luno discovery and three targeting the Tellus discovery. In the Luno area, nine of the wells are going to be production wells and three are going to be used as water alternating gas (WAG) injection wells.

The development of the Tellus area will comprise of one WAG well and two production wells. Seven of the oil producing wells are going to be horizontal in the reservoir section, with the longest estimated to be 5.5 km in length (LundinNorwayAS 2014).

3.2 Physical Understanding of Drilling Challenges Associated with the Edvard Grieg Conglomerates

During the appraisal-drilling program, harder conglomerate formations and challenging drilling conditions have proved to be a reality, both inside and below the reservoir section. Throughout the field, the tendency seems to be that below the cap rock, the reservoir comprises of very good reservoir quality sandstone. This section is further referred to as the Golden Zone. Below the Golden Zone, the tendency seems to be alternating layers between slightly coarser sands and moderately sorted conglomerate, further referred to as the Transition Zone. Below the Transition Zone follows a coarser and poorly sorted conglomerate section, containing granitic boulders, before the granitic basement formation follows. This conglomerate section is called the Conglomerate Zone. Figure 3-2 below illustrates the general lithology distribution of the field's reservoir, even though the thickness and presence of the three zones vary with location. In some of the wells, Hydrocarbons have been proven inside the upper parts of the Conglomerate Zone, as well as in the Golden Zone and the Transition Zone (Personal communication; Elseth T.).

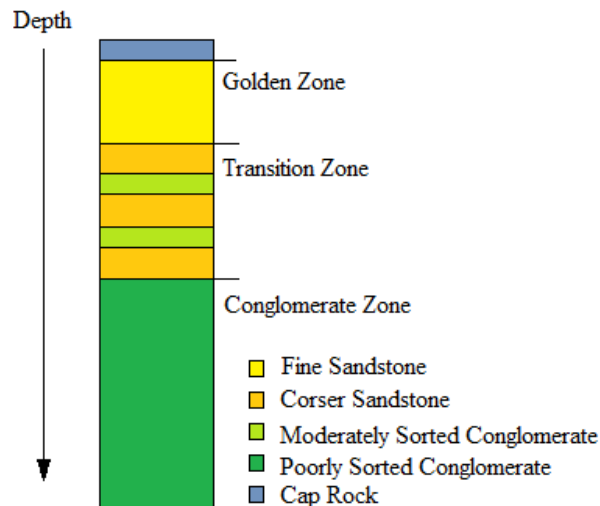


Figure 3-2: General zone classification of formations inside and surrounding the Eedvard Grieg reservoir.

Hilgedick et al. (2012) conducted triaxial tests of conglomerate cores acquired from an appraisal well at the Edvard Grieg field, to determine the unconfined compressive strength of different conglomerate types encountered during drilling. Three samples were taken and tested for two different conglomerate types, at different depths. The first conglomerate type was a weak matrix conglomerate, consisting of clasts of various sizes with a porous sandstone matrix. The second conglomerate type was strong, non-porous matrix conglomerate. When conducting the test, the vertical stress (S_1) and the horizontal stress (S_2) were recorded at failure. The results are shown in Table 3-1. Figure 3-3 shows how a Mohr-Coulomb failure criterion was constructed, to determine the UCS of the different conglomerate types. The UCS value can be found where the trend line crosses the S_1 -axis. The results show that the UCS for the weak matrix conglomerate lies just above 12 MPa and for the strong matrix conglomerate lies just below 30 MPa. From the values described in Table 2-1, both conglomerate types tested qualify as moderately strong rock.

Table 3-1: Stress results from triaxial tests of two different conglomerate samples from the Edvard Greig field. The tests were run on different core samples at 2, 5, and 10 MPa confining stress (Hellvik et al. 2012).

Material	Depth [m]	S ₁ [MPa]	S ₃ [MPa]
Weak matrix Conglomerate	1904.51	19.1	2.0
Weak matrix Conglomerate	1904.51	36.6	10.0
Weak matrix Conglomerate	1904.51	56.2	15.0
Strong Matrix Conglomerate	1969.35	29.9	2.0
Strong Matrix Conglomerate	1969.35	69.0	10.2
Strong Matrix Conglomerate	1969.35	64.5	15.4

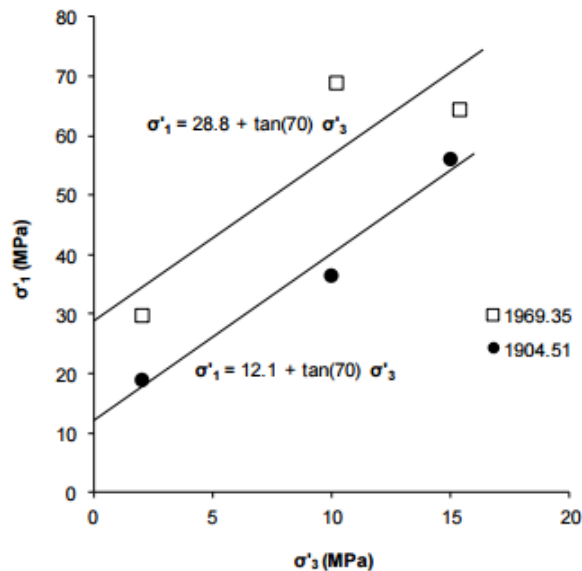


Figure 3-3: Determination of UCS from triaxial tests from two different Edvard Grieg conglomerates (Hilgedick et al. 2012)

The results from Hilgedick et al. (2012) indicates that the conglomerate samples do not show properties qualifying them to be referred to as an extremely hard rock. However, pictures of the core samples before and after the triaxial tests show that a clear failure plane cannot be identified. Failure seems to be occurring along undulated paths along the interfaces between the sandstone matrix and conglomerate clasts. See Figure 3-4. This indicates that the strength of the clasts themselves is higher than the strength of the formation in general.



Figure 3-4: Triaxial test sample from weak matrix conglomerate from the Edvard Grieg field (Hilgedick et al. 2012)

Several appraisal wells have been drilled through the conglomerates of the Edvard Grieg field at different locations. Experiences from some of the bit runs of four different appraisal wells drilling through the conglomerate are listed in Table 3-2 .

Table 3-2: Dull Bit Grading after drilling in conglomerate formations on the Edvard Grieg Field. (Bialon et al. 2010, Huse and Magnussen 2008, Johnsrud et al. 2009, Skuncke 2014)

Well	Bit type	Meters Drilled in Conglomerate	Dull Bit Grading
Well A	8 ½’’ TCI Bit	199.3	2-7-BT-H-E-2-LT-LOG
Well A	8 ½’’ PDC Bit	70	8-1-RO-N-X-I-CT-PR
Well B	8 ½’’ PDC Bit	80	7-1-RO-N-X-I-CT,BT-PR
Well B	8 ½’’ PDC Bit	262	7-1-RO-N-X-I-BT,CT,HC-PR
Well C	8 ½’’ TCI Bit	163	6-7-BT-A-E-I-L-T-TD
Well D	12 ¼’’ TCI Bit	227	4-3-WT-A-E-I-NO-TD

Today it is not uncommon that a PDC or TCI bit would be expected to drill entire sections, or up to 2-3000 m in sandstone, before needing to be changed out (Personal communication; Skalle, P. 2015; Elseth, T. 2015). In the cases listed in Table 3-2 however, some bits do not

exceed 100 m. This indicates extremely harsh drilling conditions. The dull bit grading recorded from bits that drilled through the conglomerate sections also shows extensive damage to the bit. Bit teeth were worn, chipped and broken. The two first numbers of the official IADC Dull Bit Grading system, created to compare bit damage or failure between different bit types, are describing damage to the inner and outer cutting structure respectively. The numbers range between 0 and 8, where 0 means no lost, worn and/or broken parts of the cutting structure, and 8 means 100% of cutting structure was lost, worn and/or broken, or that no usable cutting structure remains (PetroWiki 2014). For further explanation of the IADC Dull Bit Grading System, see figure in Appendix A. Experiences from Edvard Grieg are presented in Table 3-2 and show severe damage to the inner cutting structure for PDC bits, and higher, or equally high, damage on the outer structure for TCI bits.

The short amount of distance each bit is being able to drill per run inside the conglomerate formation, and the dull bit grading showing severe damage to the bits are all evidences for the conglomerate formations causing extensive drilling challenges. The combination of high formation strength of the granitic clasts and the fact that the clasts seems to loosen from the weaker sand matrix before fracturing themselves, are seen as some of the reasons why this conglomerate formation is causing these challenges. Lundin Norway AS has two theories of how the clasts and boulders complicate the drilling by damaging the bit, and a combination of the two theories is probably the case. The first theory states that when the bit is drilling through the conglomerates, the bit will rotate slowly once a cutter is grinding its way through a granitic boulder. When the same cutter leaves the boulder, and propagates into the much weaker sandstone matrix, the bit immediately speeds up. The subsequent collision between the high velocity cutter and a new, or the same, granitic boulder is thought to be so powerful that it is damaging to the cutter. If this happens continuously through the formation, the bit will gradually be worn down, and will not be able to obtain high penetration rate over time. This is also believed to be a major reason for stick slip behavior experienced in the conglomerate sections. The second theory states that since failure in the conglomerate formation occur along the interfaces between the clasts and the sandstone matrix, a pebble or a boulder can easily break out of the formation and get caught inside the inner part of the bit. If this clast is too large to be cleaned out by the jet nozzles, it will continuously impact and damage essential parts of the bit, such as cutters and nozzles. Figure 3-5 show an example of this behavior from Well A, where the bit drilled 70 m and was ringed out and lost one nozzle (Personal communication: Elseth T., Sigvartsen, E., Lembourn P.)

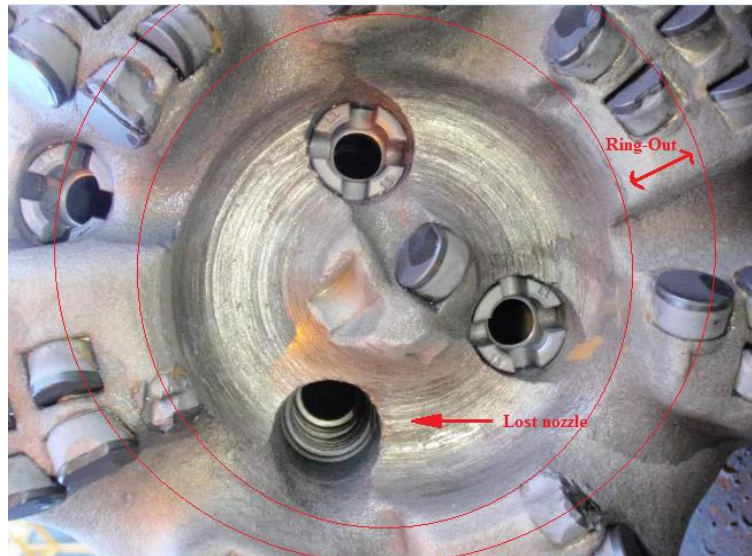


Figure 3-5: Ringed out bit and one nozzle missing after drilling through Edvard Grieg conglomerate (Hellvik et al. 2012).

Another significant challenge associated with drilling in the conglomerate is the difficulty of selecting the right drilling dynamic parameters at the right time. High formation strength of the granite clasts and boulders, compared to the lower formation strength of the surrounding sandstone matrix and the overlaying sandstone, cause rapid variation in drilling parameters while drilling through the formation. This makes it hard to optimize the parameters to the mechanical properties of the formations. The granitic clasts are also varying in size and distribution, from a couple of centimeters large pebbles to 1 m large boulders (Personal communication; Seljebotn, P. Ø). As the LWD tools used for formation evaluation can be situated from a couple to several meters behind the bit, the verification that rough drilling intervals indeed was a granitic boulder is not confirmed/disconfirmed before long after having penetrated the boulder (Nilsen 2014). For Well A, the BHA tools was located from 3 to 30 m behind the bit, while for Well B from 2 to 30 m (Bialon et al. 2010, Skuncke 2014). This can again have caused extensive bit wear by the time the formation evaluation reach the interval in question, since preventive alterations of drilling parameters was not able to be conducted real-time.

Lundin Norway AS wants to mitigate the mentioned challenges above to maintain a more efficient penetration rate drilling through the conglomerates on Edvard Grieg. The fastest possible penetration rate is not necessarily considered to be the optimal penetration rate in this kind of formation, but rather the penetration rate that can produce the longest bit runs. By optimizing the combination between bit choice and penetration rate, one would need fewer runs

when drilling long horizontal production wells during the current field development, and hence lower drilling cost. Present thesis will further study the challenge of detecting the conglomerate through drilling data logs acquired real-time, to enable instantaneous drilling parameter alterations while intercepting hard, troublesome conglomerate.

3.3 Mathematical Model of Formation Hardness

The mathematical model used in present thesis to reveal hard formations through penetration rate and drillability is Bourgoyne and Young's model presented in chapter 2.5.2. This subchapter will explain the assumptions made to simplify the equation, and account for the choices made regarding determination of empirical exponents.

3.3.1 Simplification of Model

The mathematical model of calculating drillability of present thesis is based on equation (2-13). From this, equation (2-1) was used to calculate the formation hardness.

$$ROP = (f_1)(f_2)(f_3)(f_4) \dots (f_8) \quad (2-13)$$

$$Formation\ Hardness = \frac{1}{Drillability} = \frac{1}{K} \quad (2-1)$$

The eight functional relations of drilling variables from equation (2-13) are not all assessed to influence the penetration rate, and consequently the drillability, to the same extent. Some of the functional relations are assumed to only influence the penetration rate over large spans, and are therefore assumed constant during drilling operations over short intervals. This includes the functional relations f_7 and f_8 , representing bit tooth wear and bit hydraulics respectively. The effect of compaction, given by the functional relations f_2 and f_3 , are also assumed to not have a major impact on the formation given. The functional relation of overbalance, f_4 , is assumed constant throughout every bit run.

Functional relations considered relevant for changes in penetration rate is drillability, given in equation (2-14), as well as the effect of weight on bit and rotational speed, from equations (2-18) and (2-19) respectively.

$$f_1 = e^{2.303a_1} = K \quad (2-14)$$

$$f_5 = \left[\frac{\left(\frac{WOB}{d_b}\right) - \left(\frac{WOB}{d_b}\right)_t}{4 - \left(\frac{WOB}{d_b}\right)_t} \right]^{a_5} \quad (2-18)$$

$$f_6 = \left(\frac{RPM}{60}\right)^{a_6} \quad (2-19)$$

The functional relation of drillability is determined in equation (3-1).

$$f_1 = K \quad (3-1)$$

The functional relation of weight on bit is simplified in equation (3-2).

$$f_5 = \left[\frac{\left(\frac{WOB}{d_b}\right) - \left(\frac{WOB}{d_b}\right)_t}{4 - \left(\frac{WOB}{d_b}\right)_t} \right]^{a_5} = [WOB]^{a_5} \quad (3-2)$$

The threshold bit weight is often quite small and therefore neglected in this case. All calculations of drillability will be conducted in intervals with the same bit diameter. The bit diameter is therefore neglected, since the exact number of drillability is not of interest, only relative change of drillability. The number 4 is a conversion factor, and is by the same reason as above, neglected.

The functional relation of rotary speed is simplified in equation (3-3).

$$f_6 = \left(\frac{RPM}{60}\right)^{a_6} = [RPM]^{a_6} \quad (3-3)$$

The number 60 is also a conversion factor, and can be neglected.

From the remaining functional relations that are assumed to influence penetration rate, the mathematical model is reduced to:

$$ROP = (f_1)(f_5)(f_6) = K * [WOB]^{a_5} * [RPM]^{a_6} \quad (3-4)$$

From acquired drilling data, the variables ROP, WOB and RPM are known, and an expression of drillability can be obtained by rearranging equation (3-4):

$$K = \frac{ROP}{[WOB]^{a_5} * [RPM]^{a_6}} \quad (3-5)$$

Bourgoyne and Young's model has been developed for roller cone bits. In present thesis it is assumed that the same model is valid for other bit types, such as PDC bits and core bits as well.

3.3.2 Determination of exponents

Two exponents from equation (3-5) are not previously determined from acquired drilling data for the Edvard Grieg field. In practice, Bourgoyne et al. (1986) states that it is prudent to select the best average values of a_2 to a_8 for the formation types in the depth interval of interest. However, determining the bit weight exponent, a_5 , and the rotary speed exponent, a_6 , is not straightforward. Frequent changes in lithology with depth makes it difficult to determine these exponents from a series of penetration rate measurements made at different bit weights and rotary speeds. The lithology may change before tests are completed (Bourgoyne et al. 1986).

Bourgoyne et al. (1986) claims that one way of determining the exponents a_5 and a_6 is through a drill off test. The exponents can be estimated from penetration rate measurements taken in similar formations at similar bit operations at the beginning and end of a bit run. A drill off test consists of selecting a depth where uniform lithology is expected. The break is then locked, and one determines the time it required to drill off 10% of the weight currently in use. Further, the bit weight should be increased to the initial value, at least 20% over the current bit weight. Once completed, drill at that weight long enough to establish a new bottomhole pattern. The time allowed is usually one characteristic time per 10% increase in bit weight. Then the breaks are locked again, whilst maintaining constant rotary speed. The time should be recorded every time

the bit weight falls off 4000 lbf. Continue this until at least 50% of the initial bit weight has been drilled off. A log-log plot of Δt vs W vs R is then created. For a straight-line plot, the slope should be equal to the bit weight exponent, a_5 . The rotary speed exponent, a_6 , can be obtained using penetration rates obtained at two different rotary speeds at the same bit weight (Bourgoyne et al. 1986). The two penetration rates have to be plotted on a log-log paper against the average bit weight, and the rotary speed exponent is equal to the distance between the two graphs in the parallel region (Solberg 2012).

Young (1969) has pioneered the development of a computerized drilling control system in which both the bit weight and the rotary speed could be varied systematically when a new formation type was encountered. The two exponents are automatically computed from the observed penetration rate response. Values of the bit weight exponent obtained from field data range from 0.6 for soft formations to 2 for hard formations, and for the rotary speed exponent from 0.4 for hard formations and to 1 for soft formations (Bourgoyne et al. 1986).

4 Testing of Model

A data-agent created to test whether the challenging conglomerate of the Edvard Grieg field could be detected through calculation of formation hardness, have been developed. This chapter will present available drilling data used to test the data-agent, account for the analysis made to clean up the datasets and present the data-agent itself.

4.1 Acquired Real-Time Drilling Data

Lundin Norway AS has provided real-time surface drilling data from several wells on the Edvard Grieg field. Data acquired for six wells have been available, and due to confidentiality the wells used are further referred to as well A, B, C, D, E and F. The geographic location of the six wells with respect to each other are shown in Figure 4-1. Data from well A have primarily been used to test the formation hardness calculating data-agent during the creation. After data-agent completion, data from the other five wells have been imported into the model.

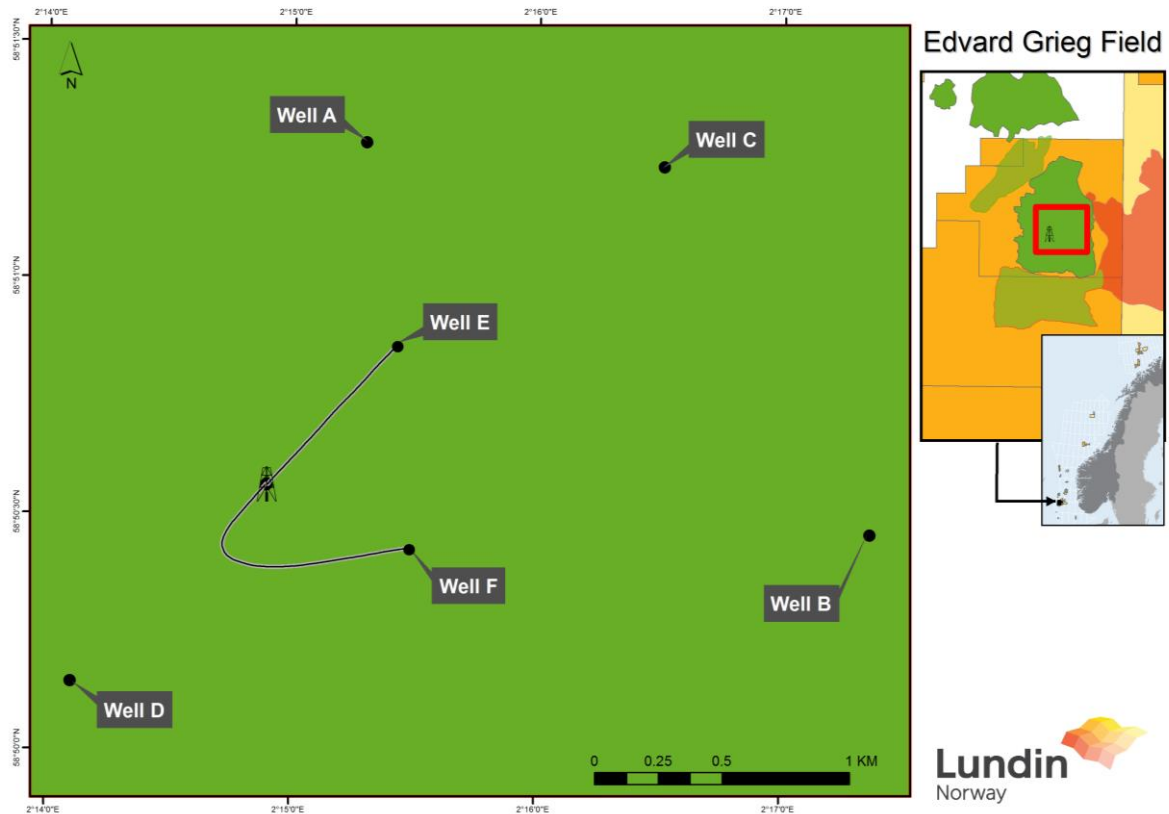


Figure 4-1: Geographic location of Well A-F, drilled on the Edvard Grieg Field (Wenum 2015).

All the acquired datasets are depth based, and thus processed by the contractors responsible for surface measurements to exclude tripping in and out of hole. For all the six wells, data acquired and processed by the mud-logging contractor have been utilized. The available datasets have provided several drilling parameters, but only parameters relevant to the mathematical model from equation (3-5) have been included in the data-agent. These parameters are penetration rate rotational speed, bit weight and depth. A method of the mud logging company's choice has been applied to calculate average ROP.

For Well A, the surface data used have a sampling rate of 6 measurements per meter, while for the Well B to Well F, the mud logging contractor have provided datasets with one sampling per meter. Data files with more samplings per meter would be preferred to be able to alter the data in a controlled manner. However, the timeframe of present thesis did not permit further investigation to acquire this.

In addition to the mud logging datasets, end of well reports, coring reports and bit records for Well A to Well D have been available. The same information accompanying Well E and Well F have not been available. These documents are currently under development due to recent drilling of the wells. Information regarding Well E and F have therefore been acquired from personal communication with Lundin Norway employees, software available at Lundin Norway AS's office and through daily drilling reports from the drilling operations. Formation evaluation data for each of the six wells was also available from the subsurface team at Lundin Norway AS, through the E&P software platform, Petrel.

4.2 Analysis of Available Data

For determining what depth intervals to examine and analyze for the different wells, intervals containing both the Golden Zone, Transition Zone and Conglomerate Zone were preferred. The intervals were specifically chosen, as changes in formation hardness was assumed to be especially evident over the transition between zones.

Well A to D were all appraisal wells, while Well E and Well F were pilot production wells. Due to Lundin Norway AS's extensive field data acquisition strategy, the interval from just above the reservoir, the reservoir itself and some distance below the reservoir have all been cored for the six wells used in present thesis. To be able to make comparisons between the six wells concerning the transition from one zone to another, the interval examined for all wells where chosen to be the cored interval. Table 4-1 show measured depth (MD) and length of the cored interval for all six wells (Bialon et al. 2010, Huse and Magnussen 2008, Johnsrud et al. 2009, Skuncke 2014). A table containing information regarding number of bit runs, core bit type, bit dull grading before and after bit run, length of bit run and formation drilled for each run is presented for all the six wells in Appendix B.

Table 4-1: Depths of coring intervals for Well A-E

Well	Start of cored interval [m MD]	End of cored interval [m MD]	Length [m]
A	1917	2000.7	83.7
B	1886	1986	100
C	1868	1987.5	119.5
D	1930	1973	43
E	2095	2183.2	88.2
F	2254.3	2327.8	73.5

To analyze formation hardness calculated by the data-agent against the actual lithology, facies logs exported from Petrel software was used. The subsurface team at Lundin Norway AS generated the facies logs based on LWD and Wireline data. These logs show the start and end depths of each formation, mostly sandstone and conglomerates, and clearly indicate the three main zones.

4.3 The Formation Hardness Detecting Data-Agent

The formation hardness detecting data-agent was created using MATLAB. Firstly, the MATLAB program imports the drilling data files and processes the data. It then uses the modified Bourgoyne and Young's (1986) mathematical model of penetration rate from equation (3-5) to calculate drillability. From this, the program uses equation (2-1) to compute the formation hardness. Finally, the program creates different plots to display the calculated formation hardness against depth. Figure 4-2 illustrates the data process flow of the MATLAB program.

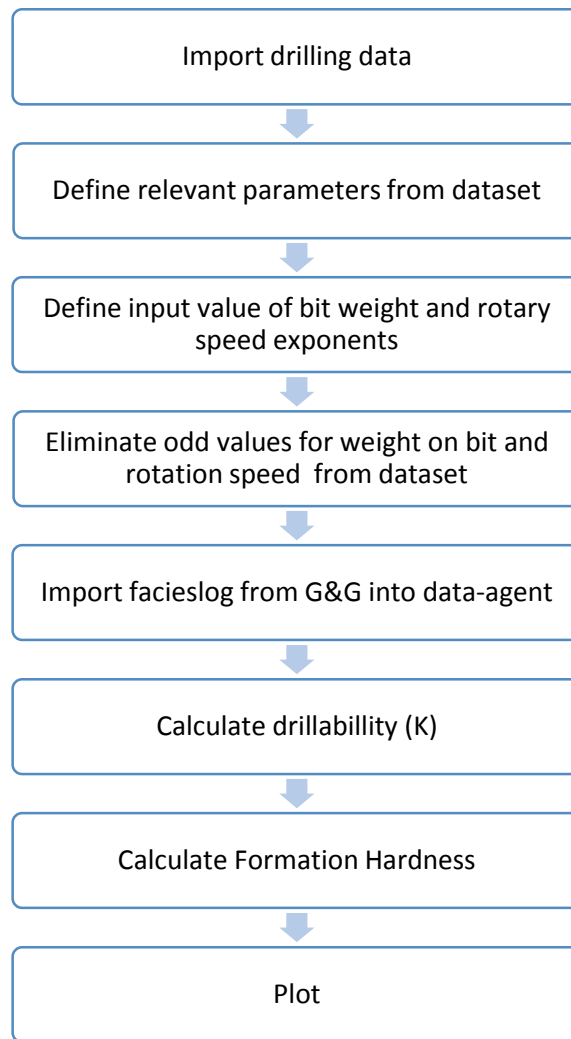


Figure 4-2: Data process flow of formation hardness detection data-agent.

The dataset available for Well A, processed by the mud logging contractors, contained several dummy values. These had to be removed to clean up the logs. The dummy values are assumed to be a measuring error, and are indicated as -999.25 in the excel files.

The column containing RPM-values contained occasional dummy values throughout. The RPM trends do not fluctuate much from element to element, since this parameter is more or less controlled by the driller. Therefore, the elements containing a dummy value were replaced with the previous element's value, to maintain the general trend through the interval.

The column containing WOB-values contained dummy values, but also non-dummy values below zero. As it is not possible to obtain negative WOB, all values below zero was excluded.

No dummy values were present for ROP, since these values were already processed by the mud logging contractor.

After removing odd values, the facies log exported from Petrel was imported manually into the MATLAB program for each well. Each formation type was assigned their own value to the corresponding correct depth; fine sandstone = 1, coarser sandstone = 2, moderately sorted conglomerate = 3, poorly sorted conglomerate = 4 and other formations = 0. A new column vector similar to the Petrel log was then created containing these new values, making up the facies log.

In present thesis, the conduction of a drill off test to determine the bit weight and rotary speed exponent, a_5 and a_6 , was not possible. First, the empirical exponents were therefore assumed to an average value. Then, the exponents were assigned a “soft formation value” and a “hard formation value”, which were to be used when creating a moving average data-agent that continuously alters the exponents when calculating formation hardness, based on the formation drilled. Table 4-2 present the numerical values for the exponents used in the data-agent.

Table 4-2: Values for bit weight and rotary speed exponents used in the data-agent.

Exponent	Average Value	Soft Formation Value	Hard Formation Value
a_5	1.3	1.1	1.5
a_6	0.7	0.8	0.6

To clean up the calculated logs the MATLAB built-in *smooth*-function was used. The function was especially helpful to detect trends in Well A, where several data points per meter made the logs busy. This function smooth the data in a column vector y by using a moving average filter, where the new values are returned in the column vector yy . The first elements of this yy column vector are given in equation (4-1) to (4-4) (MathWorks 2015).

$$yy(1) = y(1) \tag{4-1}$$

$$yy(2) = \frac{y(1) + y(2) + y(3)}{3} \quad (4-2)$$

$$yy(3) = \frac{y(1) + y(2) + y(3) + y(4) + y(5)}{5} \quad (4-3)$$

$$yy(4) = \frac{y(2) + y(3) + y(4) + y(5) + y(6)}{5} \quad (4-4)$$

5 Results

The results of running the developed data-agent will be presented in present chapter. First, the determination of bit weight and rotary speed exponents and the results of using the smooth-function are presented. Then the results of running the final data-agent on all the six wells, Well A-F, are shown. A modified data-agent that automatically alters the exponents to hard or soft values, based on the formation drilled, was tested on Well A. The results obtained from this data-agent are also presented. Finally, the calculated formation hardness in logarithmic view is compared with the known lithology for each well.

5.1 Results of Running the Hardness Detection Data-Agent

Before calculating formation hardness, all odd values and dummy-values were removed from the data sets. The average values of the bit weight exponent, a_5 , and the rotary speed exponent, a_6 , from Table 4-2 were chosen to calculate drillability for Well A to F.

The MATLAB smoothening function, described in chapter 4.3 was used to smoothen out the drilling data and formation hardness logs for visual improvement. The function calculates a moving average over the last x data points, where x is an input of the users choice. Figure 5-1 displays the results of testing the smoothening function on Well A for $x = [0 \ 3 \ 5 \ 10]$. It was decided to utilize smoothening over the last 5 points for Well A to avoid losing important trends or events in the dataset. A smoothening over the last 3 points was decided for Wells B-F, since these wells comprise of fewer data points per depth unit. The smoothening function has been used for all logs further presented.

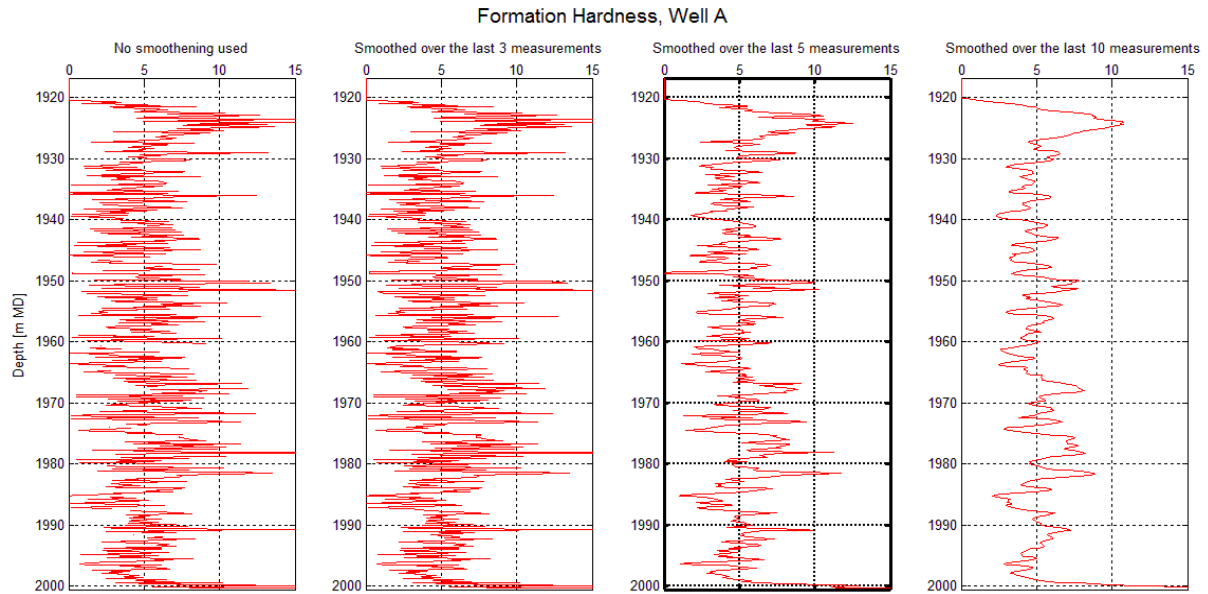


Figure 5-1: Formation hardness log for Well A, displayed with four different settings of the moving average MATLAB smoothening function. Average exponent values have been used to calculate the formation hardness. From the left: No smoothening have been used, a moving average over the last 3 acquired data points have been used, moving average over the last 5 points and moving average over the last 10 points.

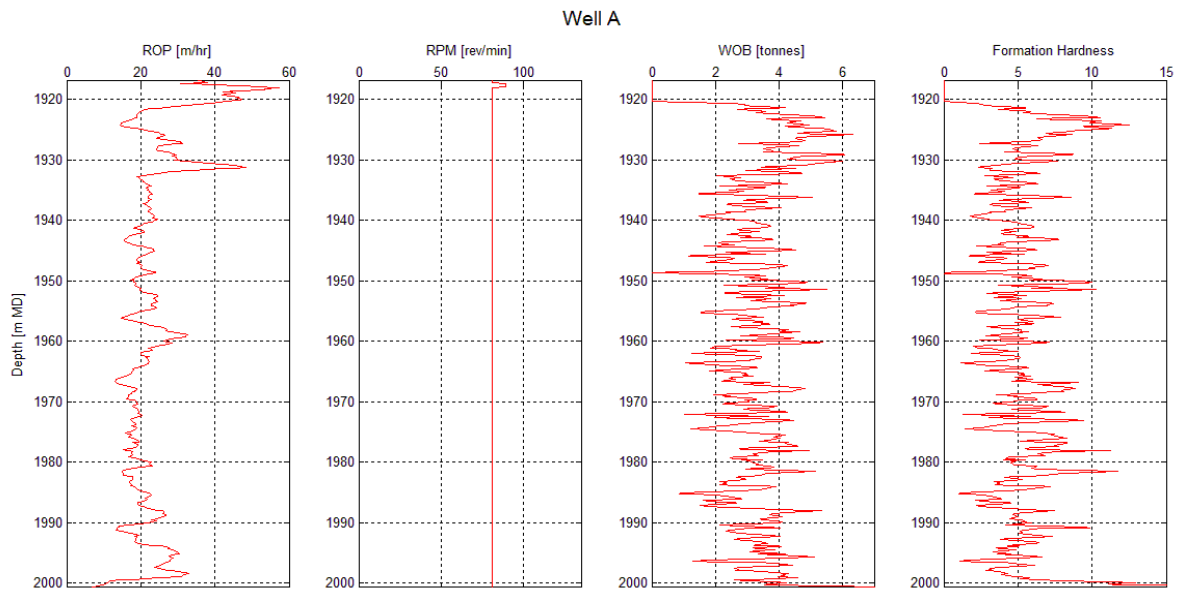


Figure 5-2: Well A. ROP, RPM, WOB and calculated Formation Hardness plotted against depth of cored 8 1/2" interval. Average exponent values ($a_5 = 1.3$ and $a_6 = 0.7$) have been used to calculate the formation hardness.

Figure 5-2 presents the calculated formation hardness results for Well A, together with the relevant drilling parameters ROP, RPM and WOB plotted against depth for the 8 ½” cored interval. Average values for the bit weight exponent and rotary speed exponent have been used. Observations are listed below:

- Generally high ROP.
- Constant RPM.
- Low, but fluctuating, WOB.
- Generally low values for formation hardness. Some high markers are observed at the approximate depths 1925 m, 1950 m, 1978 m, 1982 m, 1991 m and 2000 m. These indicate hard stringers.
- The average formation hardness from approximately 1930 m to 1965 m is slightly lower than the average trend from 1965 m to 1985 m.

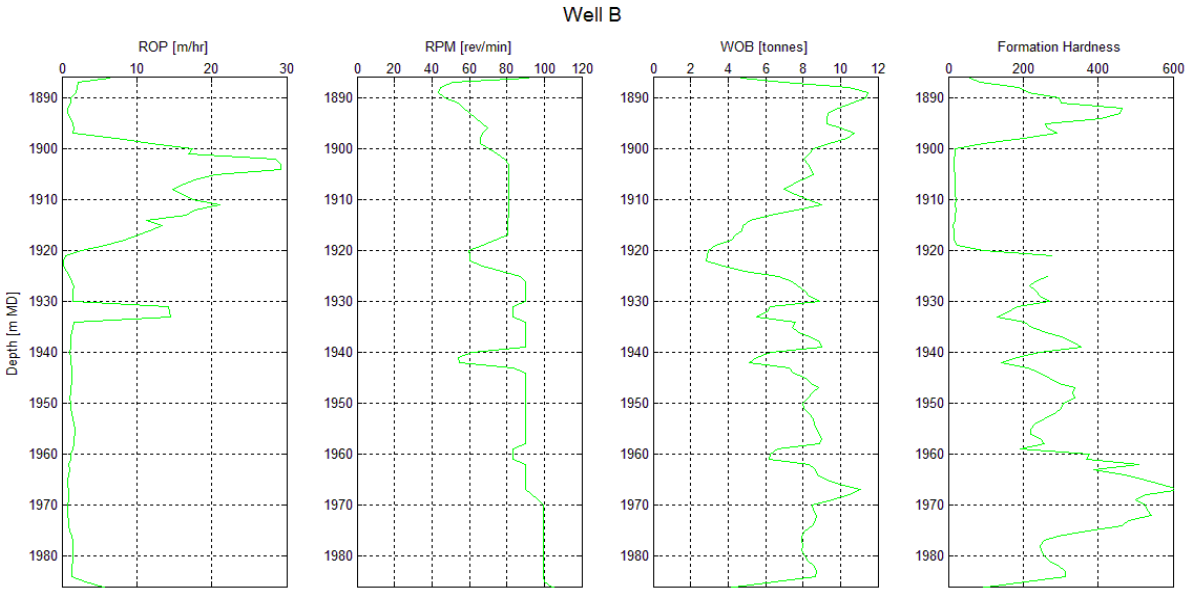


Figure 5-3: Well B. ROP, RPM, WOB and calculated Formation Hardness plotted against depth of cored 8 ½” interval. Average exponent values ($a_5 = 1.3$ and $a_6 = 0.7$) have been used to calculate the formation hardness.

The results for Well B are displayed in Figure 5-3. Formation hardness is calculated with average exponent values. Observations are listed:

- High ROP values up to 30 m/hr deviates from the much lower trend at approximately 1902 m. It peaks again at 1932 m.
- Slightly increasing RPM throughout the entire interval.

- Relatively high, but varying, WOB.
- Generally high formation hardness values (40 times the general hardness of Well A).
- A softer layer is indicated between 1900 m to 1920 m.
- High markers are observed at 1892 m and between 1960 m to 1975m. Indicates hard formations.

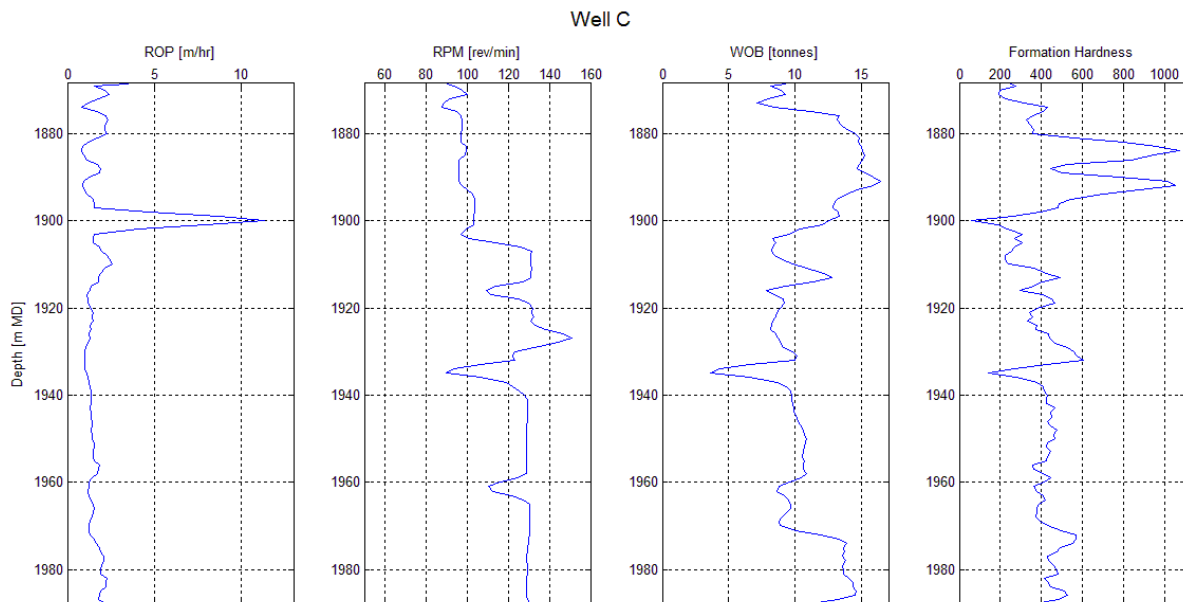


Figure 5-4: Well C. ROP, RPM, WOB and calculated Formation Hardness plotted against depth of cored 8 ½” interval. Average exponent values ($a_5 = 1.3$ and $a_6 = 0.7$) have been used to calculate the formation hardness.

Figure 5-4 presents calculated formation hardness for Well C. Average exponent values have been used. Observations are listed below:

- Low ROP. A high peak in the penetration rate is seen at 1900 m.
- Generally higher RPM than wells A and B. Starts at 100 rev/min and is increased to 125 rev/min.
- High WOB.
- High formation hardness at 1870 m, 1885 m, 1895 m, 1912 m 1918 m, 1932 m and 1972 m. Indicates hard layers.
- Softer markers indicated at 1900 m and 1935 m.

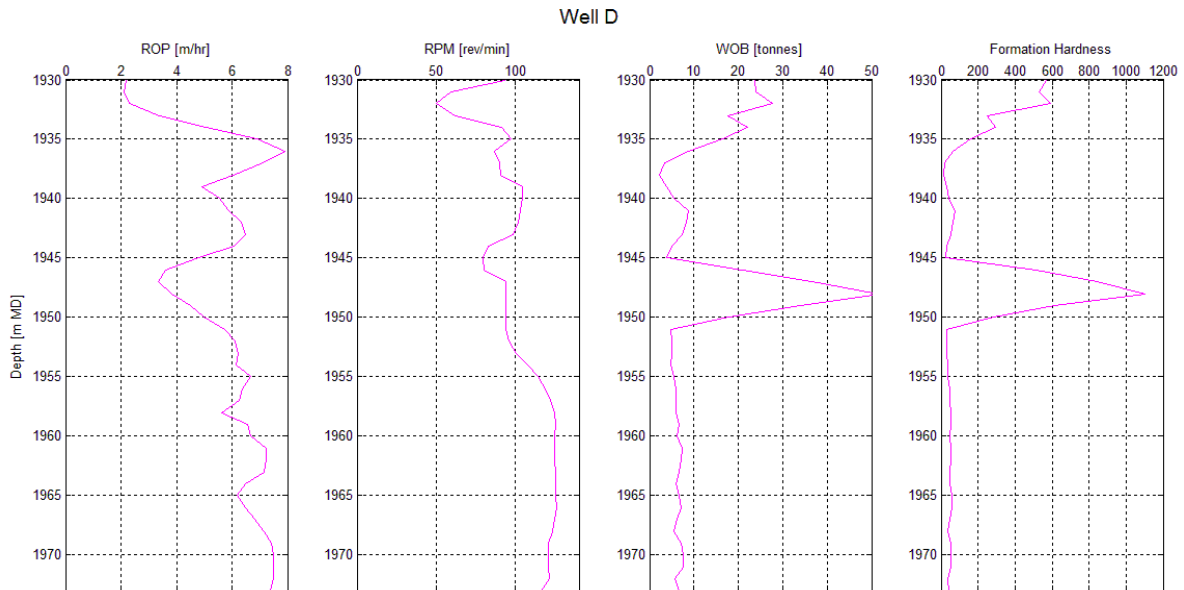


Figure 5-5: Well D. ROP, RPM, WOB and calculated Formation Hardness plotted against depth of cored 8 ½” interval. Average exponent values ($a_5 = 1.3$ and $a_6 = 0.7$) have been used to calculate the formation hardness.

Figure 5-5 displays the formation hardness results from Well D. Average exponents have been used. Observations are listed:

- Generally high ROP values.
- Increases RPM from 100 rev/min to 120 rev/min at 1955 m.
- Extreme peak in WOB at 1948 m. Generally high WOB values.
- Very high formation hardness around 1930 m and at 1948 m. Combination of high WOB and low ROP gives high formation hardness, indicating hard layers at these depths.

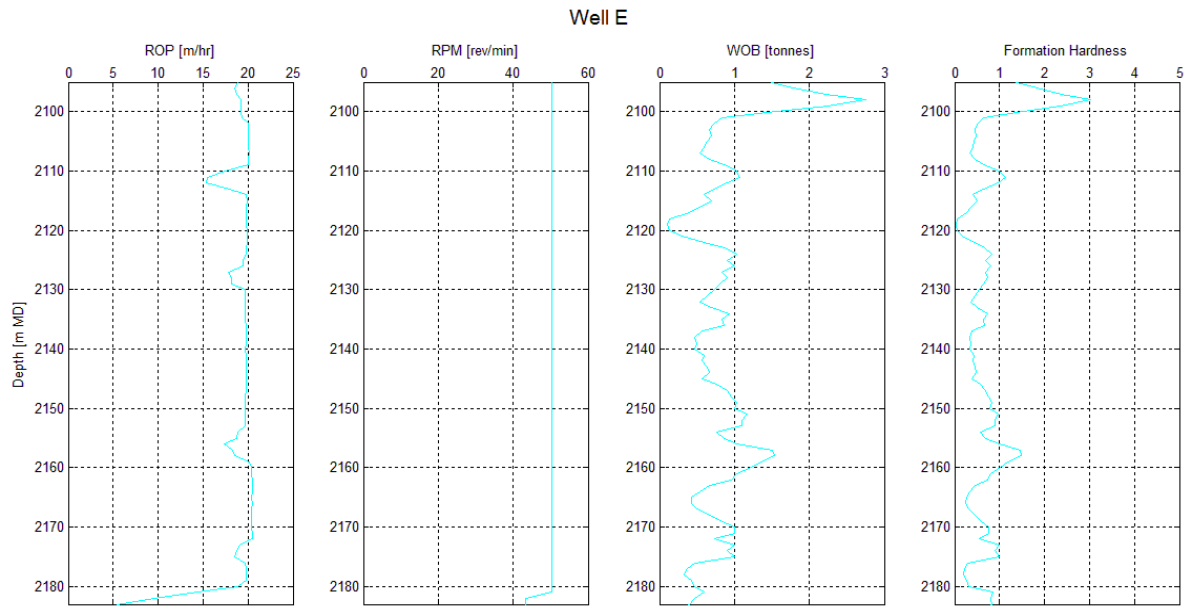


Figure 5-6: Well E. ROP, RPM, WOB and calculated Formation Hardness plotted against depth of cored 8 ½” interval. Average exponent values ($a_5 = 1.3$ and $a_6 = 0.7$) have been used to calculate the formation hardness.

The results for Well E are shown in Figure 5-6. Average exponent values have been used. This well show extremely soft formations. Observations are listed:

- High, relatively constant ROP.
- Constant lower RPM.
- Low, varying values of WOB.
- High ROP and low WOB indicates high drillability and extremely soft formations.
- Formation hardness is extremely low (1/10 of Well A). Some higher markers at 2098 m, 2110 m, 2152 m, 2158 m and 2174 m, indicating harder layers.

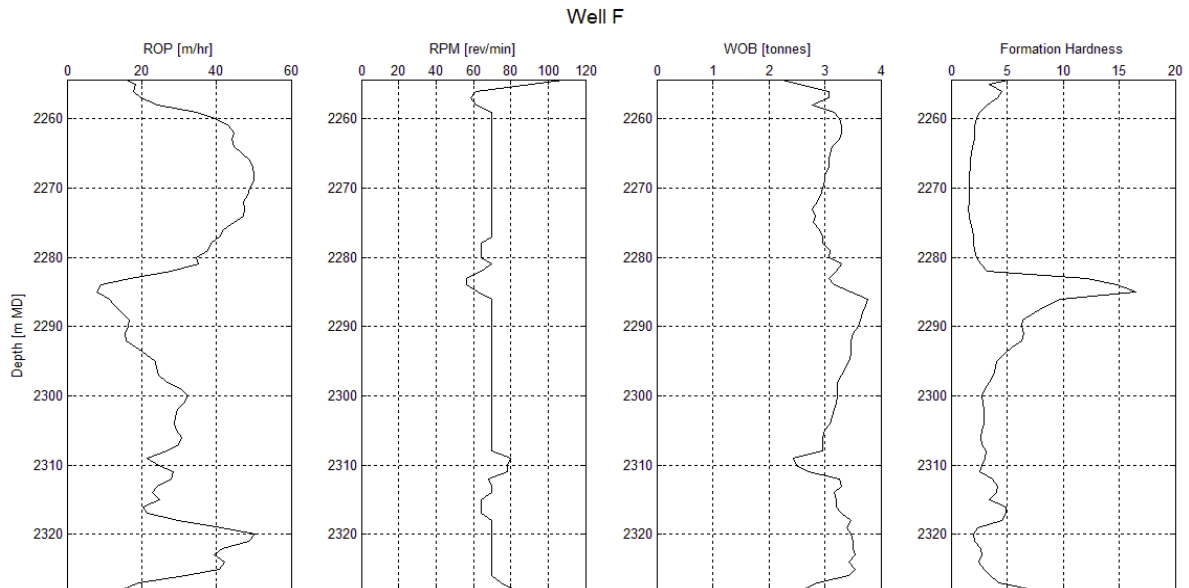


Figure 5-7: Well F. ROP, RPM, WOB and calculated Formation Hardness plotted against depth of cored 8 ½” interval. Average exponent values ($a_5 = 1.3$ and $a_6 = 0.7$) have been used to calculate the formation hardness.

The results from Well F are given in Figure 5-7. Average exponent values have been used to calculate formation hardness. Also this well had soft material. Observations are listed:

- Generally high, but largely varying ROP. Especially high penetration rate from 2250 m to 2280 m.
- Constant RPM.
- WOB varying around 3 tonnes.
- Generally low formation hardness. Higher marker observed at 2285 m and 2330 m. These depths indicate hard formations.

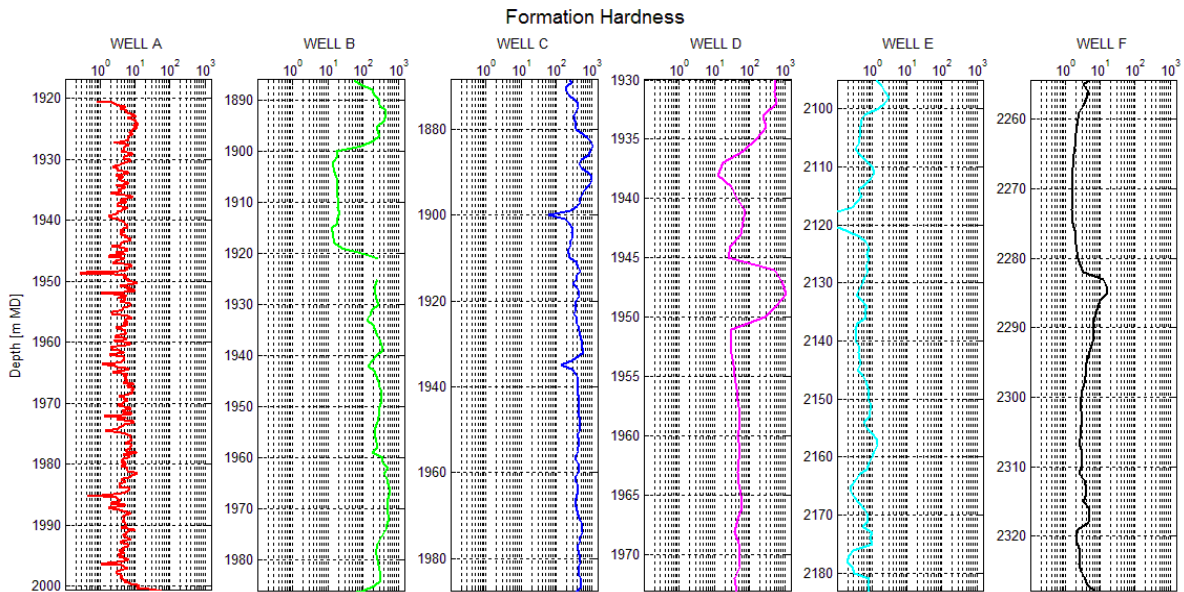


Figure 5-8: Formation hardness in logarithmic view plotted against depth for all wells, Well A-F. Average exponent values ($a_5 = 1.3$ and $a_6 = 0.7$) have been used to calculate the formation hardness.

Figure 5-8 presents the formation hardness calculated for all the wells in logarithmic view. Local variations in formation hardness are observed, where higher markers indicate hard stringers or layers. Lower values indicate soft formations. One can observe that the general formation hardness value is significantly higher for Wells B, C and D, than for Wells A, E and D. Possible reasons for variation in formation hardness values between wells are discussed in chapter 6.

Automatic adjustment of empirical model exponent constants

An attempt to create a data-agent that continuously altered the bit weight exponent and rotary speed exponent value based on local hardness was made and tested on Well A. Figure 5-9 presents the results with the blue line. To obtain this result the data-agent first calculate the formation hardness using average exponent values over the entire interval. It then runs through the drilling data set again and calculates the moving average over the last 5 data points. If the moving average times a threshold value of 10 % above its own value is higher than the calculated average, the data-agent replaces the old formation hardness value from the first round of calculations with a new value calculated using hard formation exponent values. If the moving average times a threshold value 10 % below its own value is lower than the calculated average,

the data-agents replace the old formation hardness value with a new one, using the soft formation exponent values. It is observed that the automatic shifting of exponent values enhanced the hardness function by magnifying the extremes.

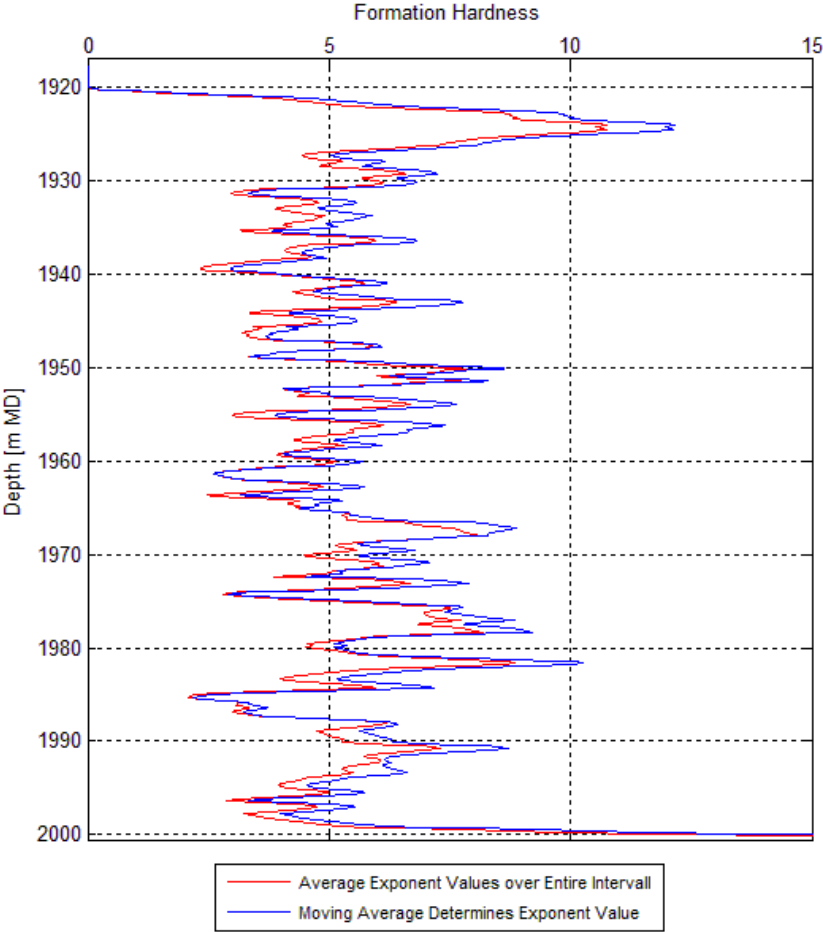


Figure 5-9: Formation hardness for Well A calculated with static exponent values and automatic changing exponent values. The red line shows formation hardness calculated by using the average exponent values ($a_5 = 1.3$ and $a_6 = 0.7$). The blue line shows formation hardness calculated by using a moving average, times a threshold value, to determine whether soft formation exponent values ($a_5 = 1.1$ and $a_6 = 0.8$) or hard formation exponent values ($a_5 = 1.5$ and $a_6 = 0.6$) should be used to calculate the formation hardness.

5.2 Comparison of Data-Agent Results with Facies Logs

Present subchapter will present the formation hardness in logarithmic view vs depth and compare it to the lithology for each well. The formation hardness values vary greatly from well to well, and a logarithmic display of the wells will make comparisons easier. Each color on the facies logs represent a specific lithology. The color scaling of the facies logs is presented in Table 5-1.

Table 5-1: Description of color scaling of facies logs for Wells A-F.

Color	Lithology Description
Dark Blue	Other Formations
Light Blue	Golden Zone Quality Sandstone
Green	Courser Sandstone
Orange	Moderately Sorted Conglomerate
Red	Poorly sorted conglomerate

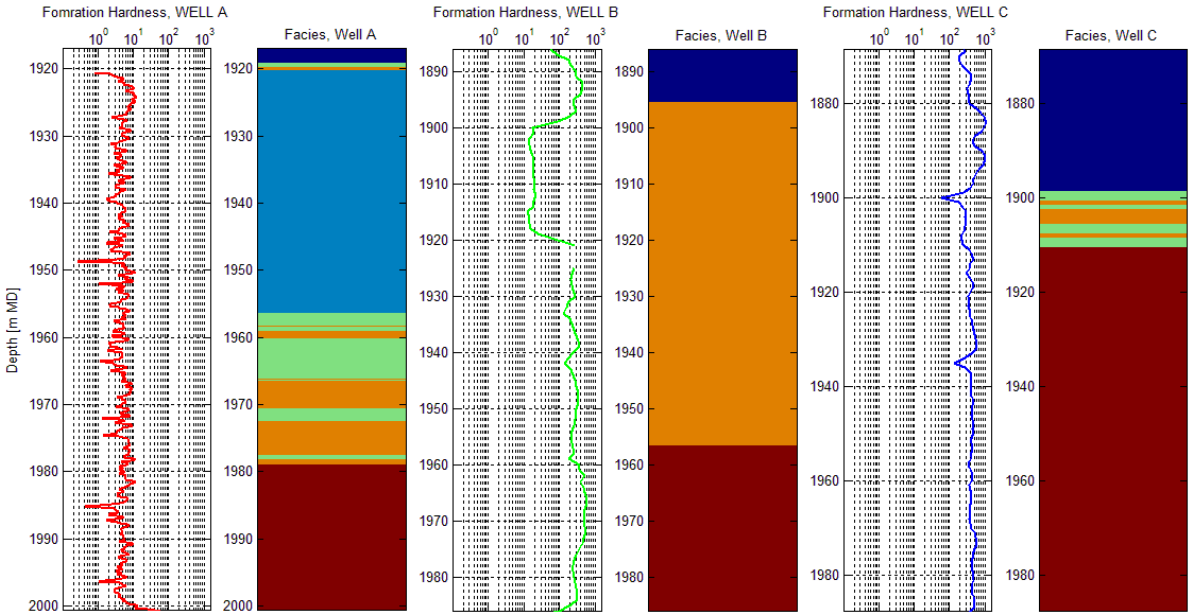


Figure 5-10: Formation Hardness plotted against depth compared to the local facies log for Wells A, B and C. Average exponent values ($a_5 = 1.3$ and $a_6 = 0.7$) have been used during calculation of formation hardness. Table 5-1 explains the color scaling of the facies logs.

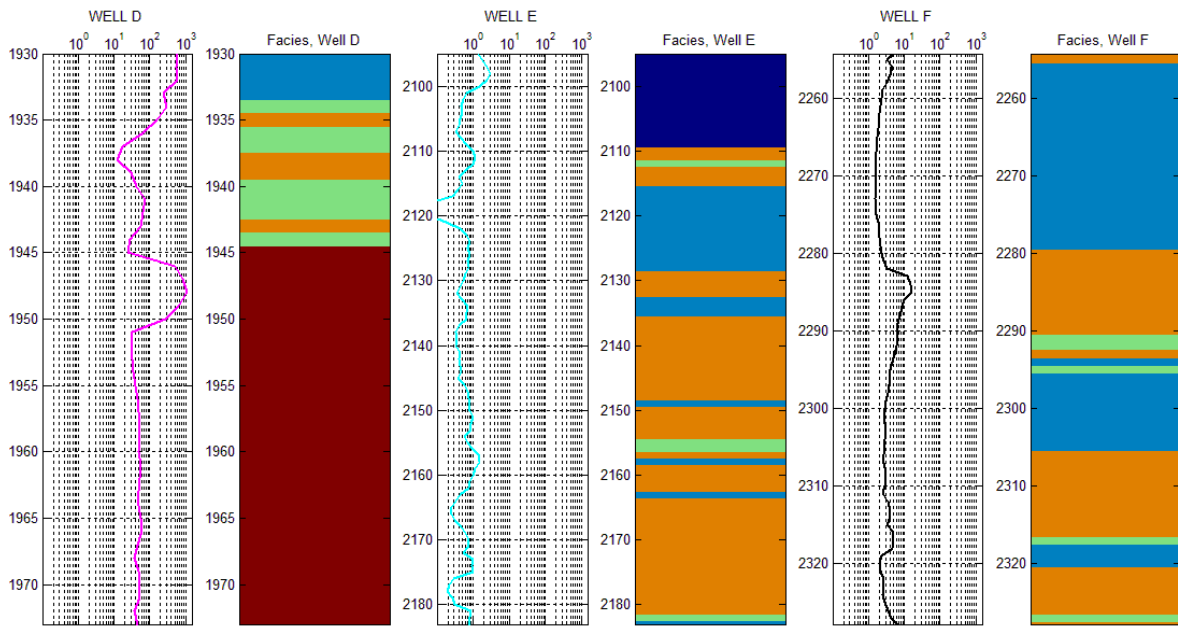


Figure 5-11: Formation Hardness plotted against depth compared to the local facies log for Wells D, E and F. Average exponent values ($a_5 = 1.3$ and $a_6 = 0.7$) have been used during calculation of formation hardness. Table 5-1 explains the color scaling of the facies logs.

From Figure 5-10 and Figure 5-11, the following observations were made:

- Well A
 - The slightly higher formation hardness observed from 1965 m to 1985 m can indicate the laminated conglomerate layers within the Transition Zone and the start of the Conglomerate Zone. The formation hardness does however go down slightly at the lower parts of the Conglomerate Zone, where the formation hardness was assumed to be at its highest.
 - Low value markers, indicating softer formation do not correspond to any observed softer layers within the conglomerate zone of the facies log.
- Well B
 - The cored interval do not drill through any sands. Only moderately and poorly sorted conglomerates.
 - The soft formation interval indicated by the formation hardness log, from 1900 m to 1920 m, is not recognized within the facies log.
 - Generally high formation hardness values across the entire cored interval, compared to Well A.

- Well C
 - The first low marker within the Transition Zone correspond to a sandstone layer.
 - The low marker within the Conglomerate Zone, indicating a soft layer, is not recognized in the facies log.
 - Extremely high formation hardness values corresponds to large amounts of the cored interval being conglomerates.
 - Would expect the formation hardness to go down within the two lower sandstone layers of the Transition Zone. The formation hardness value is slightly reduced at this point, but not as clear and significantly as expected.
- Well D
 - Only the upper moderately sorted conglomerate layer (orange) corresponds to a high marker.
 - High formation hardness values are seen within the fine sandstone layer from the facies log at the top of the interval. Conglomerate formations were expected in the facies log for these formation hardness values.
 - The low formation hardness markers do not correspond well with the sandstone layers from the facies log.
 - The highest formation hardness marker is within the Conglomerate Zone, but formation hardness is decreasing to lower values below said marker within the same conglomerates formation. An equally high formation hardness tendency was expected throughout the conglomerate zone.
 - The formation hardness is generally extremely high, even though the lithology vary greatly throughout the interval.
- Well E
 - The interval comprises mostly of moderately sorted conglomerates (orange), laminated with fine (blue) and courser (green) sandstone layers.
 - The formation hardness values are generally very low.
 - Only the upper moderately sorted conglomerate layer (orange) corresponds to a high marker (same as for Well D). Can indicate a good marker that can be recognized in other/future wells, since this is also seen for Well D.
 - The other high formation hardness markers correlate to conglomerate layers occasionally.
 - The lower formation hardness markers do not correspond very well to the sandstone layers.

- Well F
 - Low formation hardness correlate well with sandstone layers.
 - High formation hardness markers correlate with conglomerate layers occasionally.
 - More high formation hardness markers would be expected within the conglomerate layers throughout the entire interval. The formation hardness stays close to constant over some of the conglomerate layers.

Comparison of Well A and the Facies log with automatic adjustment of empirical model exponent constants

Figure 5-12 presents the same log as Figure 5-9, compared with the local lithology.

Observations made from the plot showing formation hardness calculated by using a moving average to determine the exponent values are listed:

- The upper high formation hardness markers, at 1925 m, 1942 m and 1950 m, do not correspond to the local sandstone lithology of the Golden Zone.
- The high markers within the Transition Zone does correlate to some degree with the conglomerate layers. However, not to an extent that any conclusion regarding detection of conglomerates through high formation hardness markers could be made.
- The formation hardness do not stabilize at a higher level within the Conglomerate Zone, as would be expected.
- The general trend of formation hardness value does however seem to be slightly lower in the interval between 1930 m and 1965 m, than for the interval between 1965 m and 1985 m. This could be used to recognize conglomerate rich intervals over longer runs if other wells prove the same tendency.

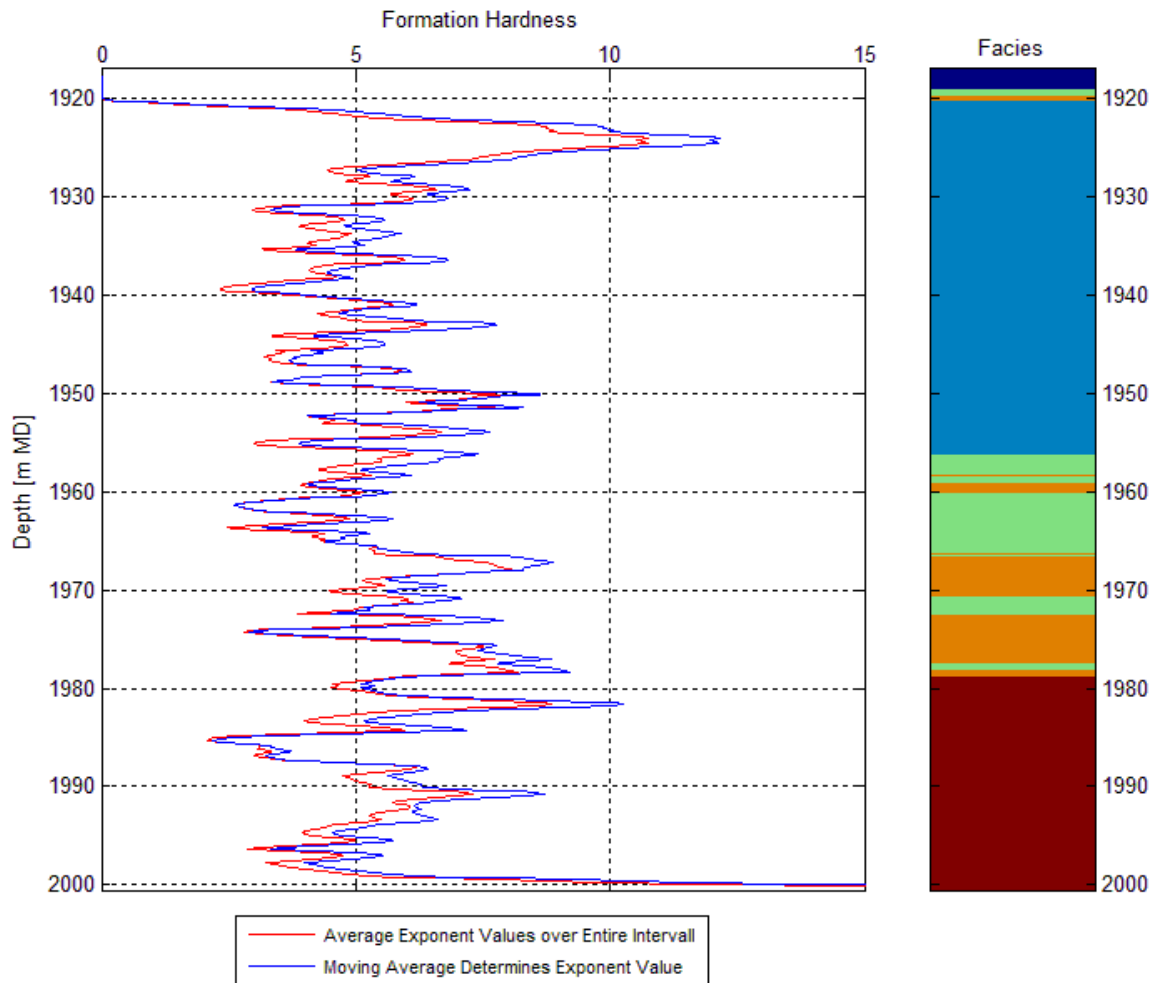


Figure 5-12: Formation Hardness compared to the local facies log for Well A. The formation hardness was calculated with average exponent values (red) and the moving average data agent determining whether to use soft ($a_5 = 1.1$ and $a_6 = 0.8$) or hard ($a_5 = 1.5$ and $a_6 = 0.6$) formation exponent values (blue).

5.3 Summary of the most helpful observations from the data-agent

- Some high formation hardness values could be used as formation markers.
- High variation in formation hardness values between wells makes it difficult to draw conclusions by well comparison.
- Better to draw conclusions for each well internally.
- No distinct formation hardness trends observed in the interface between the Golden, Transition and Conglomerate Zones.
- No distinct formation hardness difference observed in the interface between sandstone and conglomerate formations.

6 Discussion

Present thesis have estimated formation hardness through a MATLAB generated data-agent for six different wells, Well A-F, drilled on the Edvard Grieg Field. The calculation has been conducted through a simplified version of the penetration rate model proposed by Bourgoyne and Young (1986), and the relationship between drillability and formation hardness. Drilling data obtained from the mud logging contractor for each individual well has been available to calculate the formation hardness. Several assumptions and simplifications have been made to generate the data-agent. This chapter will account for the applicability of the results obtained from the data-agent, the quality of the model and assess further work to be done to improve the formation hardness detecting model of present thesis.

6.1 Applicability of Results

The goal of present thesis was to detect the challenging conglomerate formations of the Edvard Grieg field through acquired drilling data, to further enable instantaneous drilling parameter alterations, to obtain the most efficient penetration rate when intercepting the troublesome conglomerate. The applicability of the results from the hardness detecting data-agent is presented and discussed further.

Clear Tendencies from the Hardness Detection Data-Agent

Few clear tendencies have been obtained by using the data-agent on the six wells. The two most prominent tendencies are listed:

- Some high formation hardness values could be used as formation markers in future wells. The upper moderately sorted conglomerate layer in the Transition Zone is indicated by high formation hardness for both Well D and E.
- The use of an automatic moving average calculating the bit weight and rotary speed exponents for Well A, amplified the extremes of the formation hardness log.

Disappointing Lack of Tendencies from the Hardness Detecting Data-Agent

Some tendencies were expected from the data-agent, but were not observed in the results. These are listed:

- It was expected that the formation hardness would increase from softer in fine sandstone to harder in poorly sorted conglomerate, and therefore give clear indications of zonal change between the Golden, Transition and Conglomerate Zone. This was not observed.
- It was expected that when comparing the facies logs with the calculated formation hardness, high and low values of formation hardness would correspond to the conglomerate and sandstone layers respectively. This was not observed.
- Little or no variation in formation hardness within the fine sandstone of the Golden Zone was expected. However, both generally low, generally high and largely varying formation hardness values within the fine sand was observed for different wells.
- Generally high formation hardness was expected for the poorly sorted conglomerates for all wells. This was not observed consistently for all the six wells.
- The same range of formation hardness values was expected for the different formations between wells. This was not observed, as the general formation hardness was extremely high for Wells B, C and D, regardless of formation type, and much lower for Wells A, E and F.

Potential causes for Lack of Tendencies from the Hardness Detecting Data-Agent

Factors that may influence the model and potentially can cause the lack of the abovementioned tendencies are listed:

- Geological:
 - It is assumed that the conglomerates are significantly harder than sandstone. The presented results can indicate that this may not be the case.
 - It is assumed that the four categorized formation types from the exported Petrel log maintains the same geomechanical parameters throughout the entire field. The presented results can indicate that there are large variations in geomechanical properties within the same formation at other locations of the field.

- Available data:
 - The data sets used for Well B-F contain one measurement per meter drilled. Smaller geological phenomenon such as boulders or thin stringers can therefore easily appear between two data points, and escape the dataset and get lost in the formation hardness calculations.
 - The facies log exported from Petrel differentiate between four types of formations. Smaller variances inside these formations are not accounted for within the facies log. As mentioned in chapter 3.2, granitic boulders up to 1 m high have been identified within the conglomerates on Edvard Grieg, and it is assumed that these will affect the drilling. It is also assumed that the sandstone and siltstone matrix of the conglomerates will have lower formation hardness than the granitic boulders. The alternating structure of the conglomerates is not presented by the facies log, and could have explained the large variations in formation hardness within the conglomerate.

6.2 Quality of Data

The quality of the acquired data sets used to calculate formation hardness of present thesis would affect the quality of the model itself. The datasets available were generally in good condition with few dummy- and odd values. The dummy values have been removed from the datasets, and odd values for WOB and ROP have been excluded. No incidents regarding extensive measurement error have been found for the given datasets.

The dataset for Well A comprised of six data points per meter, while the datasets for Wells B-F contained one data point per meter. All datasets used for present thesis were depth based and delivered from the mud logging contractor for each individual well. The real-time raw data files acquired by the contractors were used to create the available depth based datasets. However, the data processing methods used by the mud logging contractors to calculate an average value for the different drilling parameters per meter have been unknown and was a source of error in the model.

6.3 Quality of Model

The quality of the model used in present thesis depends first of all on the goodness of the model itself, how well it account for hardness in the formation. The quality is also dependent on the simplifications and assumptions made to the mathematical model. The simplifications and assumptions made to simplify Bourgoyne and Young's (1986) mathematical model of penetration rate in present thesis are presented in chapter 3.3.1. These simplifications will, in varying degree, affect the final formation hardness results. Naturally, if fewer simplifications are made, the model will be able to give a more correct picture of real life behavior.

The bit weight and rotational speed exponents were set to a constant average value for formation hardness calculation. Comparing the results from six wells with the local facies logs for each well resulted in few clear tendencies in formation hardness between sandstone and conglomerate formations. Bourgoyne and Young's (1986) mathematical model was purposed for cone tooth bits. The range of values for the bit weight and rotary speed exponents determined by Bourgoyne and Young was in present thesis assumed to be valid for other bits and cutter types as well. This is however, a weakness in the analysis. It is assumed that the variation of the values vary significantly less when using a PDC bit or a core bit, and probably will be more directly related.

A moving average, continuously determining whether to use "hard formation exponent values" or "soft formation exponent values", was tested for Well A. This proved to magnify the extremes of the calculated formation hardness. The model was tested at a late stage within the timeframe of present thesis, and was not tested for all the six wells. It is possible that the use of such a model could have proven tendencies not shown by calculating the formation hardness, using exclusively the average exponent values.

After studying the results shown by the model, an information table with respect to bit type, bit run information and dull grading was created and examined (Appendix B). The information was analyzed to see whether core bit type and bit durability would affect the model results, as the mathematical model used do not account for mentioned variables. From the table it is observed that some of the used core bit types have been extensively worn during bit runs, while

other core bits seem more effective and do not experience any significant wearing. The bit choice and bit durability is therefore assumed to affect the model.

The inspected interval of formation hardness calculations for present model have been the cored interval of all the six wells. This particular interval was chosen because the cored interval penetrates the three different zones inside and around the Edvard Grieg reservoir more or less for all the six wells (Golden-, Transition- and Conglomerate Zone). Different types of normal core bits were used to core the intervals. None of the intervals were conventionally drilled with PDC or TCI bits. Therefore, the effects of formation change during conventional drilling have not been examined, and are left unknown.

Chapter 2.2.3. proves that vibration induced by hard formations have a significant influence on drilling performance. The effect of vibration on the penetration rate and formation hardness calculated has not been studied in present thesis, due to a restricted timeframe. However, Lundin Norway AS has in corporation with a service company conducted studies related to vibration, through down-hole drilling data acquisition, which could be used in a further study.

6.4 Future work

Present master thesis have shown that the developed data-agent, calculating drillability and formation hardness, found few clear tendencies with respect to detecting hard conglomerate formations through acquired drilling data. A further study to improve the model of detecting hard formations through real-time drilling data could include:

- Use raw time based data files. In that way, the averaging methods used to compress the datasets can be controlled, and more data points per meter can be obtained. This will reduce the uncertainty related to the datasets.
- Use less simplifying assumptions for the original Bourgoyne and Young's (1986) penetration rate model from equation (2-13) to model the reality more accurately.

- Implement, and further develop, the model using moving average to continuously determine what bit weight and rotary speed exponent constants to be used based on the formation drilled, for all wells.
- A study of the exponents used in the model should be conducted. Drill off tests, or other, should be carried out to determine the exact values of the exponent constants within the different formations of the Edvard Grieg field, for both roller cone bits, PDC bits and core bits.
- Use an improved simplified model of Bourgoyne and Young's penetration rate model, which include the effects of bit tooth wear and bit type. A new simplified model is proposed in equation (6-1). Here B_t is a variable of bit type and the functional relation of tooth wear, f_7 from equation (2-20), is included. The tooth wear exponent, a_7 , needs to be determined.

$$K = \frac{ROP}{B_t * WOB^{a_5} * RPM^{a_6} * e^{-a_7 h}} \quad (6-1)$$

- Effective vibration has a large influence on penetration rate. To improve the penetration rate model the effect of torque, torque vibration, hook load vibration and RPM-vibration both torsional and vertically should be studied and implemented into the model.
- Create a formation hardness detection data-agent based on Warren's drilling model from equation (2-4) and compare with results from the model used in present thesis, or future improved models, based on Bourgoyne and Young's penetration rate model.

7 Conclusion

Based on the results and evaluation of work in present thesis, the following conclusions are presented:

- A simplified version of Bourgoyne and Young's (1986) penetration rate model has been used to calculate drillability. Several assumptions were made to simplify the model, which contributes to a degree of error.
- A data-agent that calculates formation hardness from the simplified penetration rate model has been developed using MATLAB.
- Drilling data obtained from mud logging contractors for six different wells on the Edvard Grieg Field, delivered the relevant input parameters WOB, RPM, ROP and depth to the model.
- An average value of the bit weight and rotary speed exponents was used when calculating the formation hardness for all six wells.
- The results delivered from the data-agent showed few clear tendencies. Some high formation hardness values could possibly be used as formation markers. The assumed difference in formation hardness between fine sandstone and moderately sorted conglomerate was not proven.
- The model was not able to detect conglomerate layers or formations.
- A second formation hardness calculating data-agent was tested on Well A. This data-agent continuously used a moving average over the last five data points, to determine whether soft or hard formation exponent values should be used, based on the formation drilled.
- The results from the second data-agent proved magnification of the extremes of formation hardness calculated by the first data-agent. It did not improve the models ability to detect conglomerate layers and formations.
- Future work should focus on the mathematical model by including the effects of bit type and bit durability, determining the exponents for core- and PDC bits and determine the effects of BHA dynamic instability, induced by vibrations.

8 Nomenclature

Abbreviation	Definition
ARS	Apparent Rock Strength
ARSL	Apparent Rock Strength Log
BHA	Bottom Hole Assembly
cpf	Cost Per Foot
DEO	Drilling Efficiency Optimization
HLD	High Local Doglegs
IADC	International Association of Drilling Contractors
LWD	Logging While Drilling
MD	Measured Depth
NPT	Non-Productive Time
PDC	Polycrystalline Diamond Compact (bit)
ROP	Rate of Penetration
RPM	Revolutions per Minute
RSS	Rotary Steerable System
RTDD	Real-Time Drilling Data
UCS	Unconfined Compressive Strength
WAG	Water Alternating Gas
WOB	Weight on Bit

Parameters	Definition
a	Exponent to be determined experimentally
a, b, c	Bit constants to be determined experimentally
a_1 to a_8	Constant based on local drilling conditions
a_c, b_c, c_c	Chip hold down permeability coefficients
A_{rabr}	Relative abrasiveness
a_s, b_s	Rock strength lithology coefficients
A_v	Ratio of jet velocity

B_t	Bit type
D	True vertical depth
d_b	Bit diameter
d_n	Nozzle diameter
f_1 to f_8	Functional relations used in Bourgoyne and Young's (1986) drilling model
$f_c(P_e)$	Chip hold down function
F_j	Hydraulic impact force beneath the bit
F_{jm}	Modified impact force
g_p	Pore pressure gradient
h	Fractional tooth dullness
K	Drillability
P_e	Differential pressure
S	Rock Strength
v_f	Fluid return velocity
v_n	Jet velocity
W_c	Bit wear coefficient
W_f	Wear function
WOB_e	Effective Weight on Bit
γ_f	Fluid specific gravity
ΔBG	Change in bit tooth wear
μ	Mud plastic velocity
ρ_c	Equivalent circulation density
τ	Torque

9 Bibliography

- Alden, A. 2015. Sediment Grain Size Categories. www.about.com, http://geology.about.com/od/sediment_soil/a/sedimentsizes.htm (downloaded 26. May 2015).
- Andrews, R. J., G. Hareland, R. Nygaard et al. 2007. Methods of Using Logs to Quantify Drillability. Proc., Rocky Mountain Oil & Gas Technology Symposium, 16-18 April, Denver, Colorado, USA, Vol. SPE-106571-MS.
- Bialon, M., A. Toft, J. Bodsberg et al. 2010. Final Well Report Well A, Lysaker (10. May 2010).
- Bourgoyne, A. T. , K. K. Millheim, M. E. Chenevert et al. 1986. *Applied drilling engineering*, Vol. 2, p. 221-234. United States of America Society of Petroleum Engineers (Reprint).
- Dykstra, M. W., B. V. Schneider, J. Mota. 2011. A Systematic Approach to Performance Drilling in Hard Rock Environments. Proc., SPE/IADC Drilling Conference and Exhibition, 1-3 March Amsterdam, The Netherlands, Vol. SPE-139841-MS.
- Fiksdal, H., C. Rayton, Z. Djerfi. 2000. Application of Rotary Steerable System/PDC Bits in Hard Interbedded Formations: A Multidisciplinary Team Approach to Performance Improvement. Proc., IADC/SPE Drilling Conference, 23-25 February New Orleans, Louisiana, Vol. SPE-59110-MS.
- Fjaer, E., R.M. Holt, P. Horsrud et al. 2008. *Petroleum related rock mechanics*, 2 edition, Vol. 53, p. 55-57. Amsterdam, Elsevier (Reprint).
- Gstalder, S., J. Raynal. 1966. Measurement of Some Mechanical Properties of Rocks And Their Relationship to Rock Drillability (in *Journal of Petroleum Technology* **SPE-1463-PA**).
- Hareland, G., A. Wu, B. Rashidi et al. 2010. A New Drilling Rate Model For Tricone Bits And Its Application to Predict Rock Compressive Strength. Proc., 44th U.S Rock Mechanics Symposium and 5th U.S.-Canada Rock Mechanics Symposium, 27-30 June, Salt Lake City, Utah, Vol. ARMA-10-206.

Head, A. L. 1951. A Drillability Classification of Geological Formation. Proc., 3rd World Petroleum Congress, 28 May - 6 June, The Hague, The Netherlands, Vol. WPC-4105.

Hellvik, S., R. Nygaard, E. Hoel et al. 2012. PDC Cutter and Bit Development for Challenging Conglomerate Drilling in the Luno Field - Offshore Norway. Proc., IADC/SPE Drilling Conference and Exhibition, 6-8 March, San Diego, California, USA, Vol. SPE-151456-MS.

Hilgedick, S. A., R. Nygaard, S. Hellvik et al. 2012. Limitations of Log-Based Wellbore Stability Analysis In an Unconventional Conglomerate-Rich Reservoir In the Southern North Sea. Proc., 46th U.S. Rock Mechanics/Geomechanics Symposium, 24-27 June, Chicago, Illinois, Vol. ARMA-2012-423.

Hood, J., J. Hovden, G. Heisig et al. 2003. Real-Time BHA Bending Information Reduces Risk when Drilling Hard Interbedded Formations. Proc., SPE/IADC Drilling Conference, 19-21 February, Amsterdam, The Netherlands, Vol. SPE-79918-MS.

Hossain, M. E., A. A. Al-Majed. 2015. Fundamentals of Sustainable Drilling Engineering In: Wiley-Scrivener,
https://books.google.no/books?id=Ug99BgAAQBAJ&dq=fundamentals+of+sustainable+drilling+engineering&hl=no&source=gbs_navlinks_s (accessed 24.05.2015).

Huse, A., T. Magnussen. 2008. Final Well Report Well D, Lundin Norway AS, Lysaker (12. February 2008).

Johnsrud, P., Ø. Andersen, L. Solvang et al. 2009. Final Well Report Well C, Lundin Norway AS, Lysaker (06. May 2009).

King, H.M. 2015. Conglomerate, <http://geology.com/rocks/conglomerate.shtml> (downloaded 26. May 2015).

Lubinski, A. 1950. A Study of the Buckling of Rotary Drilling Strings. Proc., Drilling and Production Practice, 1. January, New York, New York, Vol. API-50-178.

LundinNorwayAS. 2014. Edvard Grieg, http://lundin.eyego.no/wp-content/uploads/2013/07/ot_Edvard_Grieg_05-12_e.pdf (downloaded 08. December 2014).

LundinPetroleumAS. 2014. Development - Norway - Edvard Grieg http://www.lundin-petroleum.com/eng/Development_EdvardGrieg.php (downloaded 08. December 2014).

MathWorks. 2015. Smooth. The MathWorks Inc. ,
<http://se.mathworks.com/help/curvefit/smooth.html2015>).

Mensa-Wilmot, G., B. Calhoun, V. P. Perrin. 1999. Formation Drillability-Definition, Quantification and Contributions to Bit Performance Evaluation. Proc., SPE/IADC Middle East Drilling Technology Conference, 8-10 November, Abu Dhabi, United Arab Emirates Vol. SPE-57558-MS.

Mensa-Wilmot, Graham, Martyn J. Fear. 2001. The Effects of Formation Hardness, Abrasiveness, Heterogeneity and Hole Size on PDC Bit Performance. Proc., SPE/IADC Drilling Conference, 27 February - 1 March Amsterdam, The Netherlands, Vol. SPE-67698-MS.

Nilsen, Ulrikke. 2014. Drilling Optimization of Conglomerate Reservoirs Specialization Project, Norwegian University of Science and Technology Trondheim.

Overton, Harold L. 1973. A Dimensionally Derived Rock Drillability Equation. Proc., SPE Drilling and Rock Mechanics Conference, 22-23 January, Austin, Texas Vol. SPE-4237-MS.

PetroWiki. 2015. PDC Bit Classification. Society of Petroleum Engineers
http://petrowiki.org/PDC_bit_classification (downloaded 25. May 2015 2015).

Rahimzadeh, H., M. Mostofi, A. Hashemi et al. 2010. Comparison of the Penetration Rate Models Using Field Data for One of the Gas Fields in Persian Gulf Area. Proc., International Oil and Gas Conference and Exhibition, 8-10 June, Beijing, China, Vol. SPE-131253-MS.

Santos, H., J. C. R. Placido, J. E. Oliveira et al. 2000. Overcoming Hard Rock Drilling Challenges. Proc., IADC/SPE Drilling Conference, 23-25 February New Orleans, Louisiana, Vol. SPE-59182-MS.

Schlumberger. Drillstring Vibrations and Vibration Modeling Schlumberger
http://www.slb.com/~media/Files/drilling/brochures/drilling_opt/drillstring_vib_br.pdf
(downloaded 01. November 2014).

Schlumberger. 2014. Dogleg, <http://www.glossary.oilfield.slb.com/en/Terms.aspx?LookIn=term%20name&filter=dogleg> (downloaded 26. November 2014).

Schlumberger. 2014. Keyseat, <http://www.glossary.oilfield.slb.com/en/Terms/k/keyseat.aspx> (downloaded 26. November 2014).

Schlumberger. 2014. Sedimentary, <http://www.glossary.oilfield.slb.com/en/Terms.aspx?LookIn=term%20name&filter=sedimentary> (downloaded 24. November 2014).

Schlumberger. 2014. Washout, <http://www.glossary.oilfield.slb.com/en/Terms.aspx?LookIn=term%20name&filter=washout> (downloaded 25. November 2014).

Skuncke, Nils E. ; Moe, Jakob; Lundin, Axel;. 2014. Final Well Report Well B, Lysaker (15. September 2014).

Solberg, Silje Marie. 2012. Improved drilling processes through the determination of hardness and lithology boundaries MSc, Norwegian University of Science and Technology Trondheim (May 2012).

Somerton, W. H. 1959. *A Laboratory Study of Rock Breakage by Rotary Drilling*, Vol. SPE-1163-G, American Institute of Mining, Metallurgical and Petroleum Engineers (Reprint).

Somerton, W. H., F. Esfandiari, A. Singhal. 1969. Further Studies of the Relation of Physical Properties of Rock to Rock Drillability. Proc., Drilling and Rock Mechanics Symposium, 14-15 January, Austin, Texas, Vol. SPE-2390-MS.

Standford. 2014. Some Useful Numbers on the Engineering Properties of Minerals. Stanford University <https://web.stanford.edu/~tyzhu/Documents/Some%20Useful%20Numbers.pdf> (downloaded 24. November 2014).

Thefreedictionary. 2014. Boulder. The Free Dictionary, <http://www.thefreedictionary.com/Boulder> (downloaded 24. November 2014).

Thefreedictionary. 2014. String The Free Dictionary <http://encyclopedia2.thefreedictionary.com/string> (downloaded 07. December 2014).

Wenum, E. V. . 2015. *Edvard Grieg field Well A-F*. Lysaker Lundin Norway AS (Reprint).

Wu, X., L. C. Paez, U. T. Partin et al. 2010. Decoupling Stick/Slip and Whirl To Achieve Breakthrough in Drilling Performance. Proc., IADC/SPE Drilling Conference and Exhibition, 2-4 February, New Orleans, Louisiana, USA, Vol. SPE-128767-MS.





Yin, Hongjin. 1986. Investigation On The Applications Of Statistical Formation Drillability. Proc., International Meeting on Petroleum Engineering, 17-20 March, Beijing, China, Vol. SPE-14848-MS.


Appendix A – IADC Dull Bit Grading



IADC DULL BIT GRADING									
Cutting Structure		Location	Bearings/Seals	Gage	Other Dull Char.	Reason Pulled			
Inner	Outer								
1	2	3	4	5	6	7	8		
<p>Inner Cutting Structure (1) (All Inner Rows) (For fixed cutter bits, use the inner 2/3 of the bit radius)</p> <p>Outer Cutting Structure (2) (Gage Row Only) (For fixed cutter bits, use the outer 1/3 of the bit radius)</p> <p>In columns 1 and 2 a linear scale from 0 to 8 is used to describe the condition of the cutting structure according to the following:</p> <p>Steel Tooth Bits A measure of lost tooth height due to abrasion and/or damage 0 - No Loss of Tooth Height 8 - Total Loss of Tooth Height</p> <p>Inner Bits A measure of total cutting structure reduction due to lost, worn and/or broken inserts 0 - No Lost, Worn and/or Broken Inserts 8 - All Inserts Lost, Worn and/or Broken</p> <p>Fixed Cutter Bits A measure of lost, worn and/or broken cutting structure 0 - No Lost, Worn and/or Broken Cutting Structure 8 - All of Cutting Structure Lost, Worn and/or Broken</p>		<p>Dull Characteristics (3) (Use only cutting structure related codes)</p> <p>*BC - Broken Cone BF - Bond Failure BT - Broken Teeth/Cutters BU - Bailor Up Bit *CC - Cracked Cone *CD - Cone Dragged CF - Cone Interference CT - Chipped Teeth/Cutters ER - Erosion FC - Flat Crested Wear HC - Heat Checking JD - Junk Damage *LC - Lost Cone LN - Lost Nozzle LT - Lost Teeth/Cutters</p> <p>OC - Off Center Wear PB - Pinched Bit PN - Plugged Nozzle/Flow Passage RG - Rounded Gage RO - Ring Out SD - Shrinktail Damage SS - Self Sharpening Wear TR - Tracking WO - Washed Out Bit WT - Worn Teeth/Cutters NO - No Dull Characteristics * Show cone number(s) under location (4)</p>		<p>Location (4)</p> <p>Roller Cone N - Nose Row M - Middle Row G - Gage Row A - All Rows Cone # 1 - 2 - 3</p> <p>Fixed Cutter C - Cone N - Nose T - Taper S - Shoulder G - Gage A - All Areas</p>		<p>Gage (6)</p> <p>Measure to nearest 1/16 of an inch I - In Gage 1 - 1/16" Out of Gage 2 - 2/16" Out of Gage 4 - 4/16" Out of Gage</p>		<p>Reason Pulled or Run Terminated (8)</p> <p>BHA - Change Bottom-Hole Assembly DIMF - Downhole Motor Failure DIF - Downhole Tool Failure DSF - Drilling Failure DST - Drill Stem Test DP - Drill Plug CM - Condition Mud CP - Core Point FM - Formation Change HP - Hole Problems</p> <p>LIH - Left in Hole HR - Hours on Bit LOG - Run Logs PP - Pump Pressure PR - Penetration Rates RIG - Rig Repair TD - Total Depth/Casing Depth TW - Twist Off TQ - Torque WC - Weather Conditions</p>	
		<p>Other Dull Characteristics (7) Refer to column 3 codes</p>		<p>Bearings/Seals (5)</p> <p>Non-Sealed Bearings A linear scale estimating bearing life used 0 - No Life Used 8 - All Life Used, i.e., no bearing life remaining</p> <p>Sealed Bearings E - Seals Effective F - Seals Failed N - Not Able to Grade X - Fixed Cutter Bit (Bearingless)</p>					

© Smith Bits, A Schlumberger Company

Appendix B - Core Drilling Information Table for Well A-D

Well:	A	B
Coring Company:	Halliburton	Baker Hughes
Core number:	1	1
Picture:	No Picture Available	
Corehead:	CT103	BHC309c
Start depth [MD]:	1917	1886
Meters drilled:	0.66	26
Dull grade in:	New	New
Dull grade out:	1-1-NO-A-X-I-RR-PR	5-4-BT-N-X-I-PN-PR
Formation drilled:	Marl	Sandstone
Core number:	2	2
Picture:		
Corehead:	CT103	BHC309c
Start depth [MD]:	1917.66	1912
Meters drilled:	2	8
Dull grade in:	1-1-NO-A-X-I-RR-PR	New
Dull grade out:	2-2-BT-A-X-I-CT-PR	5-3-BT-N-X-I-CT-PR
Formation drilled:	Marl/Shale/Sandstone with conglomerates	Sandstone
Core number:	3	3
Picture:	No Picture Available	
Corehead:	Ci3146C	BHC409Z
Start depth [MD]:	1919.7	1920
Meters drilled:	27	4
Dull grade in:	New	New
Dull grade out:	1-1-CT-N-X-I-RR-TD	6-5-BT-N-X-I-CT-PR
Formation drilled:	Marl/Conglomerate/Sandstone	Sandstone

Core number:	4	4
Picture:	No Picture Available	No Picture Available
Corehead:	Ci3146C	HHCS316
Start depth [MD]:	1946.7	1924
Meters drilled:	26	8
Dull grade in:	1-1-CT-N-X-I-RR-TD	New
Dull grade out:	1-1-WT-N-X-I-PN-TD	1-1-WT-A-X-I-PN-PR
Formation drilled:	Sandstone/Conglomerates	Conglomerate/Sandstone
Core number:	5	5
Picture:		No Picture Available
Corehead:	Ci3146C	HHCS316
Start depth [MD]:	1973.7	1932
Meters drilled:	27	10
Dull grade in:	1-1-WT-N-X-I-PN-TD	New
Dull grade out:	2-2-WT-A-X-I-CT-TD	1-1-WT-A-X-I-PN-PR
Formation drilled:	Conglomerated Sandstone	Conglomerate/Sandstone
Core number:		6
Picture:		No Picture Available
Corehead:		HHCS316
Start depth [MD]:		1942
Meters drilled:		18
Dull grade in:		1-1-WT-A-X-I-PN-PR
Dull grade out:		1-1-WT-A-X-I-PN-PR
Formation drilled:		Conglomerate/Sandstone

Core number:		7
Picture:		
Corehead:		HHCS316
Start depth [MD]:		1960
Meters drilled:		8
Dull grade in:		1-1-WT-A-X-I-PN-PR
Dull grade out:		1-1-WT-A-X-I-PN-PR
Formation drilled:		Conglomerate/Sandstone
Core number:		8
Picture:		
Corehead:		HHCS316
Start depth [MD]:		1968
Meters drilled:		18
Dull grade in:		1-1-WT-A-X-I-PN-PR
Dull grade out:		1-1-WT-A-X-I-PN-TD
Formation drilled:		Conglomerate/Sandstone
Well:	C	D
Coring Company:	Halliburton	Halliburton
Core number:	1	1
Picture:	No Picture Available	No Picture Available
Corehead:	CT103	DBS FC274Li
Start depth [MD]:	1868	1930
Meters drilled:	5	7
Dull grade in:	New	New
Dull grade out:	3-2-BN-N-X-IN-BU-P	0
Formation drilled:	Limestone	Sandstone/Granite

Core number:	2	2
Picture:	No Picture Available	No Picture Available
Corehead:	CT103	CT1031
Start depth [MD]:	1873	1944
Meters drilled:	18	29
Dull grade in:	New	New
Dull grade out:	3-3-WT-N-X-IN-PN-P	0
Formation drilled:	Limestone	Granite Conglomerate
Core number:	3	
Picture:	No Picture Available	
Corehead:	CT103	
Start depth [MD]:	1891	
Meters drilled:	10,5	
Dull grade in:	New	
Dull grade out:	3-3-WT-N-X-IN-CT-P	
Formation drilled:	Limestone/Sandstone	
Core number:	4	
Picture:	No Picture Available	
Corehead:	Ci3146B	
Start depth [MD]:	1901,5	
Meters drilled:	13,1	
Dull grade in:	New	
Dull grade out:	1-1-WT-A-X-IN-RR-PR	
Formation drilled:	Sandstone	
Core number:	5	
Picture:	No Picture Available	
Corehead:	Ci3146B	
Start depth [MD]:	1914,6	
Meters drilled:	19,4	
Dull grade in:	1-1-WT-A-X-IN-RR-PR	
Dull grade out:	3-4-WT-A-X-IN-PN-P	
Formation drilled:	Sandstone	

Core number:	6	
Picture:	No Picture Available	
Corehead:	Ci3146B	
Start depth [MD]:	1934	
Meters drilled:	26,5	
Dull grade in:	New	
Dull grade out:	2-2-WT-A-X-IN-RR-TD	
Formation drilled:	Sandstone	
Core number:	7	
Picture:	No Picture Available	
Corehead:	Ci3146B	
Start depth [MD]:	1960,5	
Meters drilled:	27	
Dull grade in:	2-2-WT-A-X-IN-RR-TD	
Dull grade out:	?-4-WT-A-X-IN-PN-TD	
Formation drilled:	Sandstone	

Appendix C – The MATLAB Program

```
clc
clear all

%UPLOAD DEPTHBASED DRILLING DATA FOR WELL
A=xlsread('MATLABdepthbased.xlsx');

%INPUT CONSTANTS
%Average Exponent Values
a5A=1.3;
a6A=0.7;
%Hard Formation Exponent Values
a5H=1.5;
a6H=0.6;
%Soft Formations Exponent Values
a5S=1.1;
a6S=0.8;

%RETRIEVE RELEVANT PARAMETERS FROM DATASET A
Depth=A(:,1);
ROP=A(:,13);
RPM=A(:,14);
SWOB=A(:,20);

%ELIMINATION OF DUMMY-VALUES AND ODD VALUES
%Elimination of odd RPM values
for i=1:length(RPM);
    if RPM(i)<0;
        RPM(i)=RPM(i-1);
    end
end
%Elimination of odd SWOB values
for i=1:length(Depth);
    if Depth(i)<1920.6;
        SWOB(i)=0;
    end
end
SWOB(SWOB<0)=NaN;

%IMPORT OF LOCAL FACIES LOG FOR WELL
for i=1:length(Depth);
    if Depth(i) < 1919.1;
        FaciesM(i) = 0;
    end
    if Depth(i)>= 1919.1;
        FaciesM (i) = 2;
    end
    if Depth(i)>= 1919.7;
        FaciesM (i) = 3;
    end
    if Depth(i)>= 1920.1;
        FaciesM(i) = 1;
    end
    if Depth(i)>= 1956.3;
        FaciesM(i) = 2;
    end
end
```

```

if Depth(i)>= 1958.2;
    FaciesM(i) = 3;
end
if Depth(i)>= 1958.4;
    FaciesM(i) = 2;
end
if Depth(i)>= 1959.0;
    FaciesM(i) = 3;
end
if Depth(i)>= 1960.1;
    FaciesM(i) = 2;
end
if Depth(i)>= 1966.2;
    FaciesM(i) = 3;
end
if Depth(i)>= 1966.35;
    FaciesM(i) = 2;
end
if Depth(i) >= 1966.5;
    FaciesM(i) = 3;
end
if Depth(i) >= 1970.6;
    FaciesM(i) = 2;
end
if Depth(i) >= 1972.4;
    FaciesM(i) = 3;
end
if Depth(i) >= 1977.4;
    FaciesM(i) = 2;
end
if Depth(i) >= 1978.0;
    FaciesM(i) = 3;
end
if Depth (i) >=1978.8;
    FaciesM(i) = 4;
end
end
FaciesM=FaciesM';

%CALCULATION OF DRILLABILITY
%Average Exponent values
for i=1:length(Depth);
    DrillabilityA(i)=ROP(i)/(((SWOB(i))^a5A)*((RPM(i))^a6A));
end
%Determination of Exponents by Moving Average
for i=309:length(Depth);
    DrillabilityMA(i)= ROP(i)/(((SWOB(i))^a5A)*((RPM(i))^a6A));
    if DrillabilityMA(i)>1.1*(DrillabilityMA(i-5)+DrillabilityMA(i-4)+DrillabilityMA(i-3)+DrillabilityMA(i-2)+DrillabilityMA(i-1)/5);
        DrillabilityMA(i)=ROP(i)/(((SWOB(i))^a5H)*((RPM(i))^a6H));
    end
    if DrillabilityMA(i)<0.9*(DrillabilityMA(i-5)+DrillabilityMA(i-4)+DrillabilityMA(i-3)+DrillabilityMA(i-2)+DrillabilityMA(i-1)/5);
        DrillabilityMA(i)=ROP(i)/(((SWOB(i))^a5S)*((RPM(i))^a6S));
    end
end

%CALCULATION OF FORMATION HARDNESS

```

```

%Average Exponents
for i=1:length(DrillabilityA);
    FormationHardnessA(i)=1/DrillabilityA(i);
end
FormationHardnessA=FormationHardnessA';
%Exponents Determined by Moving Average
for i=1:length(DrillabilityMA);
    FormationHardnessMA(i)=1/DrillabilityMA(i);
end
FormationHardnessMA=FormationHardnessMA';

%PLOTTING
y=Depth;
x1=ROP;
x2=RPM;
x3=SWOB;
x4=DrillabilityA;
x4_1=DrillabilityMA;
x5=FormationHardnessA;
x5_1=FormationHardnessMA;

%Figure of Drilling Parameters and Calculated Formation Hardness vs Coring Depth
figure
%ROP vs Depth
subplot(1,4,1);
plot(smooth(x1,5),y,'r');
grid on
axis([0 60 1917 2000.7]);
set(gca,'ydir','reverse','XAxisLocation','top');
xlabel('ROP [m/hr]');
ylabel('Depth [m MD]');
%RPM vs Depth
subplot(1,4,2);
plot(smooth(x2,5),y,'r');
grid on
axis([0 135 1917 2000.7]);
set(gca,'ydir','reverse','XAxisLocation','top');
xlabel('RPM [rev/min]');
%WOB vs Depth
subplot(1,4,3);
plot(smooth(x3,5),y,'r');
grid on
axis([0 7 1917 2000.7]);
set(gca,'ydir','reverse','XAxisLocation','top');
xlabel('WOB [tonnes]');
%FormationHardness vs Depth
subplot(1,4,4);
plot(smooth(x5,5),y,'r');
grid on
axis([0 15 1917 2000.7]);
set(gca,'ydir','reverse','XAxisLocation','top');
xlabel('Formation Hardness');
suptitle('well A');

%Figure of Formation Hardness Compared to the Local Facies Log
figure
%Formation Hardness vs Depth
subplot(1,2,1);

```

```

plot(smooth(x5,5),y,'r');
grid on
axis([0 15 1917 2000.7]);
set(gca,'ydir','reverse','XAxisLocation','top');
xlabel('Formation Hardness');
%Facies vs Depth
subplot(1,2,2);
imagesc(1,Depth,FaciesM);
axis([0.5 1.5 1917 2000.7]);
set(gca,'ydir','reverse','XAxisLocation','top','xtick',[]);
xlabel('Facies');
suptitle('well A');

%Figure of Calculated Formation Hardness Using Moving Average
figure
%Average Exponent Values
plot(smooth(x5,10),y,'r');
grid on
hold on
axis([0 15 1917 2000.7]);
set(gca,'ydir','reverse','XAxisLocation','top');
xlabel('Formation Hardness');
ylabel('Depth [m MD]');
%Formation Hardness Using Moving Average
plot(smooth(x5_1,10),y,'b');
hold on
axis([0 15 1917 2000.7]);
set(gca,'ydir','reverse','XAxisLocation','top');
legend('Average Exponent Values over Entire Interval','Moving Average Determines Exponent Value','Location','southoutside');

```

Published with MATLAB® R2014a